A model-based investigation of the recent rebound of shelf water salinity in the Ross Sea

Jingwei ZHANG[1], Xuebin Zhang[2], Matt A King[1], and Kewei Lyu[3]

[1]University of Tasmania
[2]Commonwealth Scientific and Industrial Research Organisation (CSIRO)
[3]Xiamen University

October 17, 2023

Abstract

Intense atmosphere-ocean-ice interactions in the Ross Sea play a vital role in global overturning circulation by supplying saline and dense shelf waters. Since the 1960s, freshening of the Ross Sea shelf water has led to a decline in Antarctic Bottom Water formation. Since the early 2010s, however, the salinity of the western Ross Sea has rebounded. This study adopts an ocean-sea ice model to investigate the causes of this salinity rebound. Model-based salinity budget analysis indicates that the salinity rebound was driven by increased brine rejection from sea ice formation, triggered by the nearly equal effects of local anomalous winds and surface heat flux. The local divergent wind anomalies promoted local sea ice formation by creating a thin ice area, while a cooling heat flux anomaly decreased the surface temperature, increasing sea ice production. This highlights the importance of understanding local climate variability in projecting future dense shelf water change.

A model-based investigation of the recent rebound of shelf water salinity in the Ross Sea

Jingwei Zhang [1,2], Xuebin Zhang[1], Matt A. King [2,3] and Kewei Lyu[4]

[1]Climate Science Centre, CSIRO Environment, Hobart, Australia

[2]School of Geography, Planning, and Spatial Sciences, University of Tasmania, Hobart, Australia

[3]The Australian Centre for Excellence in Antarctic Science, University of Tasmania, Hobart, Australia

[4]State Key Laboratory of Marine Environmental Science, College of Ocean and Earth Sciences, Xiamen University, Xiamen, China

Abstract

Intense atmosphere-ocean-ice interactions in the Ross Sea play a vital role in global overturning circulation by supplying saline and dense shelf waters. Since the 1960s, freshening of the Ross Sea shelf water has led to a decline in Antarctic Bottom Water formation. Since the early 2010s, however, the salinity of the western Ross Sea has rebounded. This study adopts an ocean-sea ice model to investigate the causes of this salinity rebound. Model-based salinity budget analysis indicates that the salinity rebound was driven by increased brine rejection from sea ice formation, triggered by the nearly equal effects of local anomalous winds and surface heat flux. The local divergent wind anomalies promoted local sea ice formation by creating a thin ice area, while a cooling heat flux anomaly decreased the surface temperature, increasing sea ice production. This highlights the importance of understanding local climate variability in projecting future dense shelf water change.

Introduction

The Ross Sea provides the densest Dense Shelf Water (DSW, the precursor for Antarctic bottom water (AABW), Figure 1a) on its continental shelf and contributes approximately 25% of all AABW formation on the Antarctic shelf (Orsi et al., 2002). Water in the western Ross Sea shelf is particularly important for AABW formation due to its high salinity, resulting from local salt inputs produced during sea ice formation (Rusciano et al., 2013; Sansiviero et al., 2017; Aulicino et al., 2018), together with remote sources advected toward the western Ross Sea by coastal currents (Assmann & Timmermann, 2005; Jendersie et al., 2018).

In the western Ross Sea, sea ice is driven northward by the persistent, strong southerly katabatic winds. During the austral winter (April- October), this results in vigorous sea ice formation and brine release, which initiates the formation of high-salinity shelf water and determines its properties (Fusco et al., 2009; Rusciano et al., 2013; Morrison et al., 2023). Moreover, the ocean circulation on the Ross Sea continental shelf consists of two main inflows from the east driven by the easterly wind, the Antarctic Coastal Current and Antarctic Slope Current (Smith Jr et al., 2012). Thus, these westward inflows are essential in transporting fresher water from the upstream Amundsen Sea to the Ross Sea (Figure 1a), influencing the long-term variability of DSW salinity in the western Ross Sea (S. Jacobs et al., 2022).

Ocean measurements in the western Ross Sea have shown a significant decrease (~0.03 psu per dec) in DSW salinity from 1958 to 2008 (Jacobs & Giulivi, 2010), which is thought to be driven by enhanced Antarctic melting in the Amundsen Sea (Nakayama et al., 2014). Beginning in the early 2010s, however, the DSW salinity in the western Ross Sea experienced a sharp rebound, with values in 2018 comparable to those in the mid-late 1990s (Castagno et al., 2019). This salinity rebound contradicts the expectation that the ongoing increased ice-sheet mass loss in West Antarctica would continue to decrease rather than increase DSW salinity in the western Ross Sea (Jacobs & Giulivi, 2010). Silvano et al. (2020), based on in situ observations, linked this salinity recovery to the enhanced sea ice formation driven by weakened easterly winds from the Amundsen Sea. However, insufficient observations limit a more comprehensive analysis of the individual physical interactions among the atmosphere, ocean, and sea ice that influence salinity variations in the western Ross Sea. In this work, we used a well-tuned global ocean sea-ice model and designed perturbation experiments to isolate the response of shelf water salinity to various atmospheric forcing, aiming to unravel the cause of observed salinity rebound. Our study highlights the importance of integrating observational data with model studies.

2 Model and experiment design

2.1 In situ hydrographic data

The observational data used in this study were sourced from in-situ salinity observations by Castagno et al. (2019), covering the period from 1995 to 2018 with sampling during most summers within this period. Hydrographic measurements in Terra Nova Bay (defined by 74.25°–75.50° S, 163°–166° E) with station depths deeper than 800 m have been used. The region chosen is representative of DSW conditions in the western Ross Sea with a marked rebound since the early 2010s (Figure 1b, red line). To compare with observations, model results are sampled in the same area for those years in which the observation data were taken (Figure 1b black line).

2.2 Model description

We adopted the Australian Community Climate and Earth System Simulator – Ocean Model 2 (ACCESS-OM2) (Kiss et al., 2020) with a configuration of 1-degree horizontal resolution and 50 z^* vertical levels covering from the surface to 5363.5m depth. The atmospheric forcing derived from JRA55-do (Tsujino et al., 2018), including wind speed, air temperature and humidity, radiation, precipitations, and sea level pressure, are used to diagnose air–sea fluxes (wind stress, heat flux, and freshwater flux) through bulk formulae and interactive coupling between ocean and sea ice. Freshwater flux and heat flux are defined as positive downward (i.e., freshwater/heat gain by the ocean). In this study, ACCESS-OM2 is initialized from a state of rest, with temperature and salinity fields coming from the World Ocean Atlas 2013 v2 monthly climatology (WOA13; (Locarnini et al., 2013; Zweng et al., 2013)).

After a 200-year spin-up under repeated 1990-1991 JRA55-do forcing (Tsujino et al., 2018), the model reached quasi-equilibrium and was then forced with the 3-hourly JRA55-do interannual year forcing for 29 years from 1 January 1990 to 31 December 2018. Our analysis focuses on the recent period 2000–2018. In this study, we used annual data from both model simulations and observations to ensure a consistent comparison between the two of them. More detailed information on the model setup can be found in the Supporting Information.

2.3 Surface salinity budget analysis

To quantify the processes driving surface salinity anomalies in our simulation, we use the surface salinity budget terms diagnosed in the model. At the surface, the ocean salinity budget in a grid cell is given by:

$$\frac{\partial S}{\partial t} = -\nabla \cdot (\boldsymbol{u}S) + \nabla \cdot (K_{eddy}S) + \nabla \cdot (K_{small}S) + \frac{(E-P-R)S}{h} + \frac{\rho_I I(S-S_I)}{\rho_0 h} \quad (1)$$

where S is sea surface salinity, $\partial S/\partial t$ is the salinity tendency, h is the grid cell thickness, and **u** is the three-dimension velocity. K_{eddy} is the diffusion tensor for mesoscale mixing, and K_{small} represents vertical diffusion and other mixing processes smaller than eddies. E and P are the rates of evaporation and precipitation (positive upward), and R is river runoff and meltwater from Antarctica and Greenland. I is the rate of sea ice formation while S_I is sea ice salinity. ρ_o and ρ_I are the reference seawater density and sea ice density, respectively.

In ACCESS-OM2 model, ocean salt content is conserved in each grid cell within the expected numerical precision. The salinity budget in Eq. 1 states that the time tendency of salinity (left-hand side) equals all contributing terms (right-hand side), including salt convergences due to the oceanic processes (advection, the first term, and diffusion, the second and third term), evaporation minus precipitation, runoff and meltwater, and sea ice. We use these salinity budget terms to isolate the respective contributions of these processes to the salinity rebound in our perturbation experiment.

2.4 Experiment design

In this study, we designed three perturbation experiments to investigate the role of atmospheric forcing in the rebound of shelf water salinity in the western Ross Sea (Table in the Supporting Information). In the first experiment, the All-Vary experiment, the ACCESS-OM2 model is forced with prescribed atmospheric conditions taken from the JRA55-do 3-hourly forcing from 2010 to 2018. In the second experiment from 2010 to 2018, the Wind-Vary experiment, the wind forcing is the same as in the All-Vary experiment, and the rest of the atmospheric forcing is replaced by the 3-hourly climatological forcing (derived over the 2000-2010 base period). In the third experiment from 2010 to 2018, the All-Fixed experiment, all the atmospheric forcing is replaced by the climatological forcing (derived over the 2000-2010 base period). In ACCESS-OM2, the ocean and sea ice models are forced by the surface heat flux, freshwater flux, and wind stress calculated on-the-fly from prescribed atmospheric conditions and model states. The ongoing increased Antarctic meltwater is not expected to explain the observed rapid salinity rebound (Adusumilli et al., 2020). Other freshwater flux, including precipitation, evaporation, and runoff, has a minimal impact on the salinity in the western Ross Sea (Jacobs & Giulivi, 2010; Porter et al., 2019).

Therefore, changes in atmospheric forcing in the study region, are mainly from surface heat flux and wind stress. We then compared the Wind-Vary experiment versus the All-Fixed experiment to isolate the impact of wind stress and compared the All-Vary experiment versus the Wind-Vary experiment to isolate the shelf water salinity response to surface heat flux anomaly.

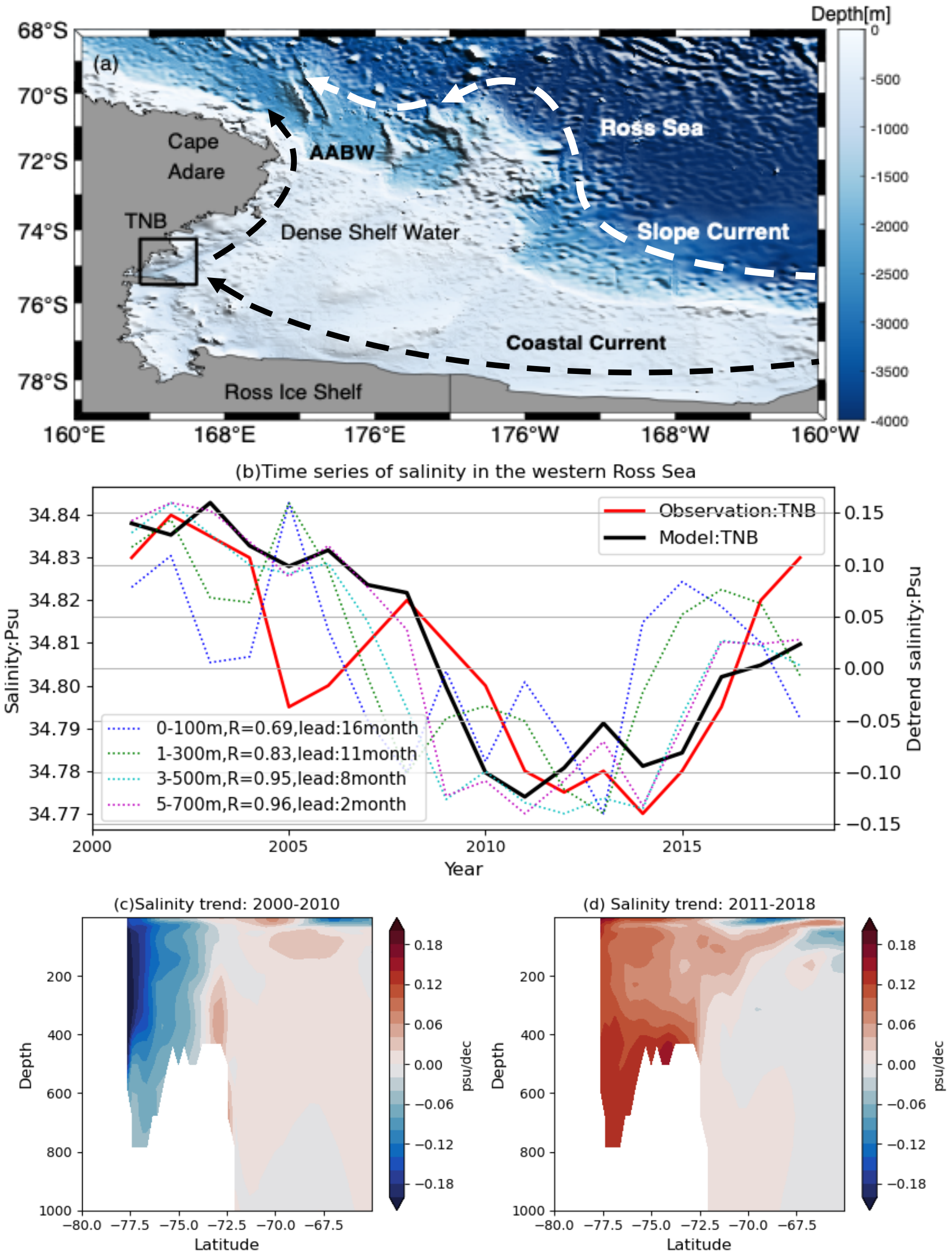

Figure 1 | Recent Recovery of DSW salinity in the Wester n Ross Sea. **(a)** Map of the Ross Sea and the study area in Terra Nova Bay (TNB, solid box). Bottom topography (m) is shown in color (Amante & Eakins, 2009). White and black dashed lines represent the general currents along the shelf break and on the shelf, referred to Smith et al. (2014). (**b**) Time series of averaged DSW salinity measured (solid red line) and simulated (solid black line) near the seafloor, as well as detrended model simulations at different depth ranges from surface to 700 m (dashed lines) and their leading correlations with salinity near the seafloor. Simulated zonal-averaged salinity trends from 2000-2010 (**c**) and 2011-2018 (**d**).

3. Results

3.1 Observed salinity variations in the western Ross Sea reproduced by model simulations

Figure 1 shows the map of the study area, and the observed and modelled salinities over different depth ranges in the western Ross Sea. The decreasing trend of DSW salinity near the seafloor before the early 2010s is estimated to be -0.05 psu/dec (Figure 1b, red line), slightly larger than the long-term trend of -0.03-0.04 psu/dec estimated by Jacobs et al. (2002) and Jacobs and Giulivi (2010). However, after reaching a minimum in the early 2010s, the freshening trend appears to reverse with a rapid salinity rebound (Figure 1b, red line). The DSW salinity in Terra Nova Bay (TNB) had rebounded up to 2018, reaching its value in the mid-late 1990s, indicating a recent recovery of DSW salinity in the western Ross Sea (Castagno et al., 2019). The observed decrease of DSW salinities between 2000 and the early 2010s followed by the sharp rebound is reproduced well by our model simulation based on ACCESS-OM2 (Figure 1b, red and black lines).

This recent sharp salinity rebound is simulated throughout the entire water column from surface to the bottom (Figures 1b, 1c,1d, and Figure S1 in Supporting Information), supported by a strong correlation, with surface salinity leading seafloor salinity at a maximum of 16 months ($r = 0.69$, $p<0.05$). We then discuss the drivers of the recent DSW salinity rebound since the early 2010s based on our model simulation.

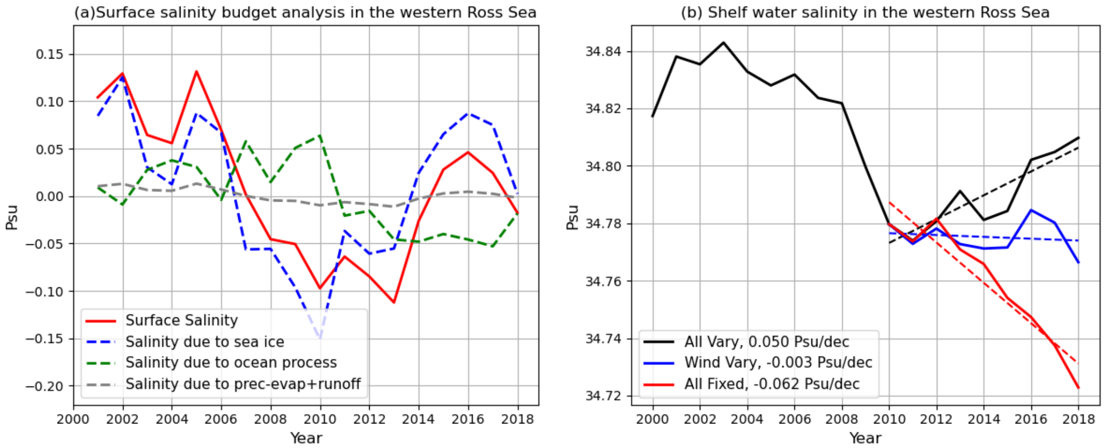

Figure 2 | Recent Recovery of DSW salinity induced by atmospheric forcing. (**a**) Time series of detrended model simulated surface salinity (red line) in western Ross Sea (162°E-168°E, 74°S-78°S), and time integrated surface salinity changes due to sea ice (bule line), net precipitation plus runoff (grey line) and oceanic process (green line) from 2000 to 2018. (**b**) Time series of averaged DSW salinity simulated by All Vary (black line) from 2000 to 2018, Wind Vary (blue line) and All Fixed (red line) and their trends (dashed lines) from 2011 to 2018 near the seafloor in TNB. Trend values are given in the legend in Psu per decade.

3.2 The effects of atmospheric forcing on recent salinity rebound through sea ice formation

A surface salinity budget analysis based on our model simulation (Figure 2a) reveals that increased brine rejection from sea ice production largely drives the recent salinity rebound over the western Ross Sea between 2010 and 2018. Oceanic processes counteract the salinity tendency implied by sea ice brine rejection. Other freshwater sources, such as precipitation minus evaporation, runoff, and Antarctic meltwater, exert minimal impact and cannot explain the observed rapid DSW salinity rebound. This is substantiated by hydrographic measurements that neither support a reduced net precipitation over the Ross Sea continental shelf (Porter et al., 2019) nor evidence of a decline in freshwater inflow from the Amundsen Sea (Adusumilli et al., 2020).

To further determine which atmospheric forcing is responsible for the recent salinity rebound, we conduct three perturbation experiments: All-Fixed, Wind-Vary, and All-Vary (see Table in Supporting Information). In the All-Fixed experiment, with atmospheric forcing remaining fixed to its climatology from 2000 to 2010, a negative trend in the salinity of the DSW is simulated (-0.062 psu/dec from 2011 to 2018, red line in Figure 2b), which is roughly consistent with the declining trend observed from the 1990s to the early 2010s (Jacobs & Giulivi, 2010; Castagno et al., 2019). The All-Fixed experiment suggests that a continued decrease in DSW salinity would be expected in the absence of changes in atmospheric conditions. The Wind-Vary experiment suggests that incorporating real-time wind forcing could basically stop the gradual decrease trend in salinity observed previously over 2000-2010 and stabilize without any obvious trends over 2010-2018 (blue line in Figure 2b). It is important to note that besides wind stress, other atmospheric factors also play a role in sea ice formation. Sea ice formation is closely connected to surface air temperature and sea surface temperature, which, in turn, is influenced by various types of surface heat flux from the atmosphere (Turner et al., 2015; Alekseev et al., 2022).

The All-Vary experiments provide compelling evidence that including all the real-time atmospheric forcing results in a notable rebound in DSW salinity in the western Ross Sea of +0.050 psu/dec over 2010- 2018, close to observations (Figure 2b, black line). Therefore, our model experiments suggest that the dynamic effect (sea ice formation driven by wind stress anomaly) and thermodynamic effect (sea ice formation driven by surface heat flux anomaly) have comparable impacts on the recent rebound in DSW salinity, contributing ~ 0.050 psu/dec each to the rebound (Figure 2b).

We next show the processes and mechanisms that how wind forcing (as revealed by comparing Wind-Vary and All-Fixed experiments) and surface heat flux (as revealed by comparing All-Vary and Wind-Vary experiments) cause increased sea ice production that further induces the recent rebound of DSW salinity in the western Ross Sea.

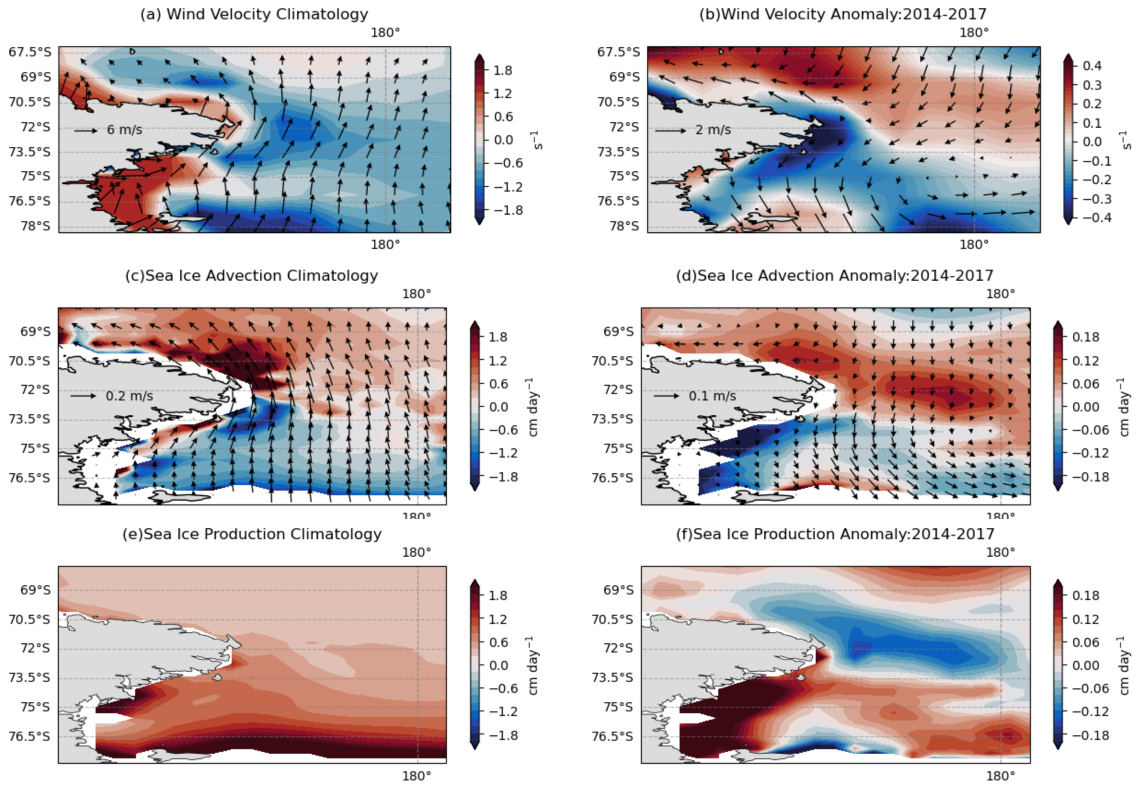

Figure 3 | Increased sea ice production due to sea ice divergence induced by wind anomalies. Climatology and 2014-2017 anomalies of winds (**a**,**b**, vectors, with colour shading represents wind divergence; negative values denote divergent), sea advection [-∇•**u**h)] (**c**,**d**, sea ice motion and sea ice mass advection), and sea ice production (**e**,**f**) induced by wind forcing.

3.3 Increased sea ice formation driven by anomalous wind forcing

Sea ice dynamical processes, such as a changed sea ice motion in response to changing surface wind stress, play an important role in the redistribution of sea ice (Holland & Kwok, 2012; Turner et al., 2015). Ice motion is described by ice velocity, whereas sea ice advection is described here by sea ice convergence [-∇• (**u**h)] (Figures 3c and 3d), where **u** is sea ice velocity and h is sea ice thickness (Zhang et al., 2010). Thus, changes in ice thickness (mass gain or loss) due to ice advection quantitatively describe the impact of wind-driven ice motion on sea ice spatial redistribution.

Mass loss due to sea ice advection generally occurs in the south region of the western Ross Sea, and ice gain occurs in the north (Figure 3c), indicating a sea ice motion from south to north in the Western Ross Sea (Comiso et al., 2011; Holland & Kwok, 2012; Turner et al., 2015). Such a sea ice advection pattern is attributed to strong northward ice motion driven by the coastal currents and strong southerly winds prevailing in winter (Holland & Kwok, 2012; Turner et al., 2016). During the period of 2014-2017, however, a local wind stress anomaly in the western Ross Sea displayed a divergent pattern (Figure 3b, blue shading). This anomaly had a notable impact on the motion of sea ice, particularly in impeding its northward motion, resulting in ice loss in the western Ross Sea (Figure 3d, blue shading, change in ocean circulation is negligible in our Wind-Vary experiment) and concurrent ice gain in the Ross Sea polynya near the coast (Figure 3d, red shading). Consequently, local changes in ice thickness (gain and loss) due to this reduced northward ice transport can be up to 0.2 cm/day, leading to the expansion of a larger area of thin ice in the north and a narrow area of thick ice near the coast (Figure S4). This increased presence of thin ice contributes to enhanced ice growth and brine rejection (Figure 3f), as growth rates of thin ice are higher compared to thick ice (Zhang et al., 2010).

The significant negative spatial correlation between the simulated anomalies of sea ice advection and sea ice production (Figures 3d, 3f, $r = -0.73$, $p<0.01$) further highlights the close relationship between wind-driven sea ice mass advection and ice production. Additionally, the sea ice loss (gain) resulting from sea ice mass advection exhibits a significant correlation with the wind divergence anomaly over the western Ross Sea (Figures 3b and 3d, $r = 0.67$, $p<0.01$). These findings suggest that, in the Wind-Vary experiment, wind forcing plays a dominant role in the formation of ice in the Ross Sea, primarily through ice mass advection processes. To identify the region where the wind forcing is responsible for the changes in sea ice in the Western Ross Sea, we conducted further experiments (Supporting Information 1.4 and Figure S2). Our investigation reveals that only when applying real-time wind forcing in the western Ross Sea region (160°E-170°W, 60°S-80°S) the model is able to successfully simulate the increased salinity of DSW driven by wind (Figures S2 and S3). This suggests that the wind-driven component of the simulated increase in DSW salinity is primarily driven by local wind anomalies rather than non-local wind originating from distant regions. Thus, during the period of 2014-2017, the amplified sea ice production and brine rejection observed in the Wind-Vary experiment in the western Ross Sea can be attributed to the thinning of sea ice caused by local divergent wind anomalies.

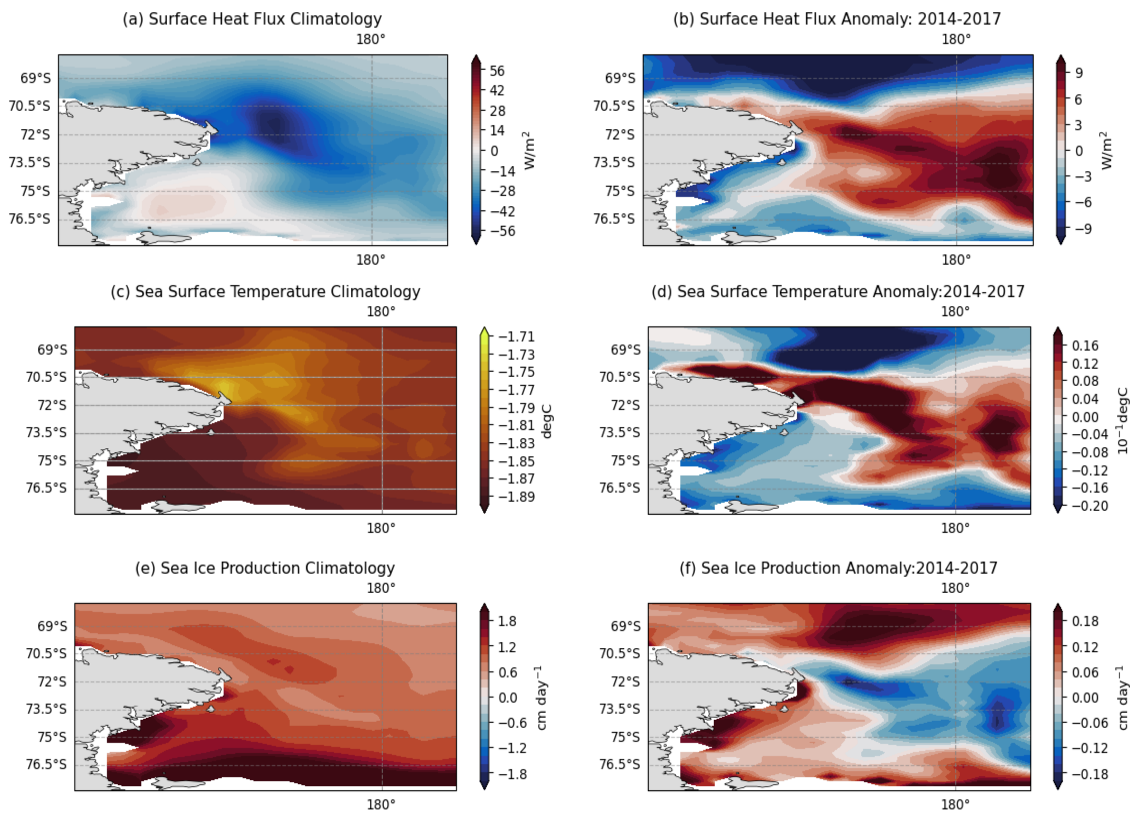

Figure 4 | Increased sea ice production due to lower temperatures induced by surface heat flux anomalies. Climatology and 2014-2017 anomalies of surface heat flux (Wm^{-2}; positive downward) (**a,b**), sea surface temperature (°C) (**c,d**) and sea ice production (cm/day) (**e,f**) induced by atmospheric forcing other than wind.

3.4 Increased sea ice formation driven by surface heat flux

In addition to the dynamical processes induced by wind, thermodynamic processes can also play an important role in the production of sea ice. During the sea ice growth season, the surface heat flux plays a crucial role in influencing sea ice production by affecting the sea surface temperature (Turner et al., 2015; Alekseev et al., 2022). During the period of 2014-2017, a comparison between All-vary and wind-vary model experiments reveals that with a decrease in surface heat flux from the atmosphere, there is a corresponding decrease in upper-ocean temperature (Figures 4b and 4d) in the western Ross Sea. This decrease in temperature promotes an increase in sea ice growth, resulting in increased brine rejection from the new ice and subsequently contributing to an increased salinity from surface to seafloor in the western Ross Sea (Figures 2b and 4f). The significant spatial correlation between the anomalies of surface heat flux and sea surface temperature (Figures 4b and 4d, $r = 0.68$, $p<0.01$), and sea ice production (Figures 4b and 4f, $r = 0.63$, $p<0.01$) further highlights the strong connection between surface heat flux and sea ice production.

It is essential to note that contrary to a simplistic inverse correlation, the relationship between sea surface temperature and net sea ice production is more intricate (Zhang, 2007). Our simulations indicate that in the upper 200 meters of the western Ross Sea, an increase in salinity and a decrease in temperature lead to increased ocean density (Figure S5). This increased upper-ocean density in turn reduces stratification (the denser layer above the lighter layer) and enhances vertical heat exchange, leading to a greater upward ocean heat transport available to melt the sea ice (Zhang, 2007; Turner et al., 2015). The pivotal balance of sea ice thus lies between the initial sea ice growth driven by surface cooling and the sea ice melt induced by vertical heat flux from the subsurface. In line with this, our model exhibits a positive anomaly in local net ice production of 0.2 cm/day (Figure 4f), primarily driven by a more pronounced increase in ice growth compared to ice melt (Figure S6). Hence, the overall increase in net sea ice production and brine rejection due to the thermodynamic process is driven by the rate of ice growth—induced by lower surface temperatures— surpassing the rate of ice melt, which itself is influenced by increased convective overturning and resultant upward ocean heat transport.

4. Discussion and conclusions

This study presents results from a model study of the recent rebound of DSW salinity in the western Ross Sea. Sea surface salinity budget analysis shows that the recent salinity rebound is dominated by increased brine rejection from sea ice formation, which further propagates and extends the whole water column from surface to seafloor (0-900 m). We further conduct three model perturbation experiments and find that this increased sea ice formation is driven by the combined effect of anomalous local wind stress and surface heat flux, which have nearly equal impacts on shelf water salinity rebound through dynamic and thermodynamic processes. During 2014-2017, the local wind anomalies induced a divergent motion in sea ice, reducing sea ice thickness and promoting local sea ice formation. Meanwhile, cooling heat flux anomaly from the atmosphere cools the surface, increasing sea ice production in winter.

The Southern Oscillation Index (SOI) captures variability associated with the ENSO events, influencing the low-pressure system over the Amundsen Sea (Amundsen Sea Low, ASL) through the atmospheric teleconnection (Lee & Jin, 2023). A negative SOI (corresponding to an El Niño event) over 2014-2017 (Figure S7a) influenced an eastward and northward shift of the ASL central (Figure S7b) (Raphael et al., 2016), leading to a reduction in the meridional sea level pressure gradient in the western Ross Sea (Figures S7 c,d) (Coggins & McDonald, 2015), thus weakening southerlies and reducing surface heat flux in the western boundary (Clem et al., 2017), ultimately leading to the recent rebound of DSW salinity through sea ice formation.

Long-term observations have recorded a freshening AABW over the past 60 years (Jacobs & Giulivi, 2010; Silvano et al., 2018), as a result of increased Antarctic meltwater (Lago & England, 2019; Johnson, 2022). Our study reveals that climate variability can temporally counteract this long-term freshening by enhancing sea ice formation and brine rejection. Future climate projections show an increased frequency of extreme El Niño events due to the greenhouse warming (Cai et al., 2014), therefore possibly enhancing AABW formation that potentially offsets or even surpasses the meltwater-induced freshening on different time scales. Thus, the experiment design and salinity budget analysis conducted here provide an essential reference for identifying the major drivers of the shelf water salinity variations from interannual to decadal time scales.

Acknowledgments

This research was supported by the Australian Research Council Special Research Initiative, the Australian Centre for Excellence in Antarctic Science (Project Number SR200100008), and the Centre for Southern Hemisphere Oceans Research (CSHOR), jointly funded by the Commonwealth Scientific and Industrial Research Organisation (CSIRO, Australia) and the Qingdao National Laboratory for Marine Science and Technology (QNLM, China). This research was undertaken with the assistance of resources from the National Computational Infrastructure (NCI Australia). The authors thank the Consortium for Ocean-Sea Ice Modelling in Australia (COSIMA; http://www.cosima.org.au) for making the ACCESS-OM2 suite of models available at https://github.com/COSIMA/access-om2.

Data Availability Statement

The observational data used in this study were sourced from in-situ salinity observations by Castagno et al. (2019), covering the period from 1995 to 2018. The model source code is available from https://github.com/COSIMA/access-om2/. The configuration files for the repeat year forced simulation are available from https://github.com/COSIMA/1deg_jra55_ryf and for the interannually forced simulation from https://github.com/COSIMA/1deg_jra55_iaf Mode experiment and outputs are available from the Zenodo repository at https://doi.org/10.5281/zenodo.8415955

Reference

Adusumilli, S., Fricker, H. A., Medley, B., Padman, L., & Siegfried, M. R. (2020). Interannual variations in meltwater input to the Southern Ocean from Antarctic ice shelves. *Nature Geoscience, 13*(9), 616-620.

Alekseev, G., Vyazilova, A., & Smirnov, A. (2022). Influence of Sea Surface Temperature in the Tropics on the Antarctic Sea Ice during Global Warming. *Journal of Marine Science and Engineering, 10*(12), 1859.

Amante, C., & Eakins, B. W. (2009). ETOPO1 arc-minute global relief model: procedures, data sources and analysis.

Assmann, K. M., & Timmermann, R. (2005). Variability of dense water formation in the Ross Sea. *Ocean Dynamics, 55*(2), 68-87.

Aulicino, G., Sansiviero, M., Paul, S., Cesarano, C., Fusco, G., Wadhams, P., & Budillon, G. (2018). A new approach for monitoring the Terra Nova Bay polynya through MODIS ice surface temperature imagery and its validation during 2010 and 2011 winter seasons. *Remote Sensing, 10*(3), 366.

Cai, W., Borlace, S., Lengaigne, M., Van Rensch, P., Collins, M., Vecchi, G., et al. (2014). Increasing frequency of extreme El Niño events due to greenhouse warming. *Nature Climate Change, 4*(2), 111-116.

Castagno, P., Capozzi, V., DiTullio, G. R., Falco, P., Fusco, G., Rintoul, S. R., et al. (2019). Rebound of shelf water salinity in the Ross Sea. *Nature communications, 10*(1), 1-6.

Clem, K. R., Renwick, J. A., & McGregor, J. (2017). Large-scale forcing of the Amundsen Sea low and its influence on sea ice and West Antarctic temperature. *Journal of Climate, 30*(20), 8405-8424.

Coggins, J. H., & McDonald, A. J. (2015). The influence of the Amundsen Sea Low on the winds in the Ross Sea and surroundings: Insights from a synoptic climatology. *Journal of Geophysical Research: Atmospheres, 120*(6), 2167-2189.

Comiso, J. C., Kwok, R., Martin, S., & Gordon, A. L. (2011). Variability and trends in sea ice extent and ice production in the Ross Sea. *Journal of Geophysical Research: Oceans, 116*(C4).

Fusco, G., Budillon, G., & Spezie, G. (2009). Surface heat fluxes and thermohaline variability in the Ross Sea and in Terra Nova Bay polynya. *Continental Shelf Research, 29*(15), 1887-1895.

Holland, P. R., & Kwok, R. (2012). Wind-driven trends in Antarctic sea-ice drift. *Nature Geoscience, 5*(12), 872-875.

Jacobs, & Giulivi. (2010). Large multidecadal salinity trends near the Pacific–Antarctic continental margin. *Journal of Climate, 23*(17), 4508-4524.

Jacobs, Giulivi, & Mele, P. (2002). Freshening of the Ross Sea during the late 20th century. *Science, 297*(5580), 386-389.

Jacobs, S., Giulivi, C., & Dutrieux, P. (2022). Persistent Ross Sea freshening from imbalance West Antarctic ice shelf melting. *Journal of Geophysical Research: Oceans, 127*(3), e2021JC017808.

Jendersie, S., Williams, M. J., Langhorne, P. J., & Robertson, R. (2018). The density‐driven winter intensification of the Ross Sea circulation. *Journal of Geophysical Research: Oceans, 123*(11), 7702-7724.

Johnson, G. C. (2022). Antarctic Bottom Water Warming and Circulation Slowdown in the Argentine Basin From Analyses of Deep Argo and Historical Shipboard Temperature Data. *Geophysical Research Letters, 49*(18), e2022GL100526.

Kiss, A. E., Hogg, A. M., Hannah, N., Boeira Dias, F., Brassington, G. B., Chamberlain, M. A., et al. (2020). ACCESS-OM2 v1. 0: a global ocean–sea ice model at three resolutions. *Geoscientific Model Development, 13*(2), 401-442.

Lago, V., & England, M. H. (2019). Projected slowdown of Antarctic bottom water formation in response to amplified meltwater contributions. *Journal of Climate, 32*(19), 6319-6335.

Lee, H.-J., & Jin, E. K. (2023). Understanding the delayed Amundsen Sea low response to ENSO. *Frontiers in Earth Science, 11*, 1136025.

Locarnini, R., Mishonov, A., Antonov, J., Boyer, T., Garcia, H., Baranova, O., et al. (2013). World Ocean Atlas 2013, Volume 1: Temperature in: NOAA Atlas NESDIS 73 edited by S. In: Levitus.

Morrison, A. K., Huneke, W. G., Neme, J., Spence, P., Hogg, A. M., England, M. H., & Griffies, S. M. (2023). Sensitivity of Antarctic shelf waters and abyssal overturning to local winds. *Journal of Climate*, 1-32.

Nakayama, Y., Timmermann, R., Rodehacke, C. B., Schröder, M., & Hellmer, H. H. (2014). Modeling the spreading of glacial meltwater from the Amundsen and Bellingshausen Seas. *Geophysical Research Letters, 41*(22), 7942-7949.

Orsi, A. H., Smethie Jr, W. M., & Bullister, J. L. (2002). On the total input of Antarctic waters to the deep ocean: A preliminary estimate from chlorofluorocarbon measurements. *Journal of Geophysical Research: Oceans, 107*(C8), 31-31-31-14.

Porter, D. F., Springer, S. R., Padman, L., Fricker, H. A., Tinto, K. J., Riser, S. C., et al. (2019). Evolution of the seasonal surface mixed layer of the Ross Sea, Antarctica, observed with autonomous profiling floats. *Journal of Geophysical Research: Oceans, 124*(7), 4934-4953.

Raphael, M. N., Marshall, G., Turner, J., Fogt, R., Schneider, D., Dixon, D., et al. (2016). The Amundsen Sea low: Variability, change, and impact on Antarctic climate. *Bulletin of the American Meteorological Society, 97*(1), 111-121.

Rusciano, E., Budillon, G., Fusco, G., & Spezie, G. (2013). Evidence of atmosphere–sea ice–ocean coupling in the Terra Nova Bay polynya (Ross Sea—Antarctica). *Continental Shelf Research, 61*, 112-124.

Sansiviero, M., Maqueda, M. M., Fusco, G., Aulicino, G., Flocco, D., & Budillon, G. (2017). Modelling sea ice formation in the Terra Nova Bay polynya. *Journal of Marine Systems, 166*, 4-25.

Silvano, A., Foppert, A., Rintoul, S. R., Holland, P. R., Tamura, T., Kimura, N., et al. (2020). Recent recovery of Antarctic Bottom Water formation in the Ross Sea driven by climate anomalies. *Nature Geoscience, 13*(12), 780-786.

Silvano, A., Rintoul, S. R., Peña-Molino, B., Hobbs, W. R., van Wijk, E., Aoki, S., et al. (2018). Freshening by glacial meltwater enhances melting of ice shelves and reduces formation of Antarctic Bottom Water. *Science Advances, 4*(4), eaap9467.

Smith Jr, W. O., Sedwick, P. N., Arrigo, K. R., Ainley, D. G., & Orsi, A. H. (2012). The Ross Sea in a sea of change. *Oceanography, 25*(3), 90-103.

Smith, W. O., Dinniman, M. S., Hofmann, E. E., & Klinck, J. M. (2014). The effects of changing winds and temperatures on the oceanography of the Ross Sea in the 21st century. *Geophysical Research Letters, 41*(5), 1624-1631.

Tsujino, H., Urakawa, S., Nakano, H., Small, R. J., Kim, W. M., Yeager, S. G., et al. (2018). JRA-55 based surface dataset for driving ocean–sea-ice models (JRA55-do). *Ocean Modelling, 130*, 79-139.

Turner, J., Hosking, J. S., Bracegirdle, T. J., Marshall, G. J., & Phillips, T. (2015). Recent changes in Antarctic sea ice. *Philosophical Transactions of the Royal Society A: Mathematical, Physical and Engineering Sciences, 373*(2045), 20140163.

Turner, J., Hosking, J. S., Marshall, G. J., Phillips, T., & Bracegirdle, T. J. (2016). Antarctic sea ice increase consistent with intrinsic variability of the Amundsen Sea Low. *Climate Dynamics, 46*, 2391-2402.

Zhang, J. (2007). Increasing Antarctic sea ice under warming atmospheric and oceanic conditions. *Journal of Climate, 20*(11), 2515-2529.

Zhang, J., Woodgate, R., & Moritz, R. (2010). Sea ice response to atmospheric and oceanic forcing in the Bering Sea. *Journal of Physical Oceanography, 40*(8), 1729-1747.

Zweng, M., Reagan, J., Antonov, J., Locarnini, R., Mishonov, A., Boyer, T., et al. (2013). World Ocean atlas 2013. Vol. 2. Salinity. NOAA Atlas NESDIS 74. In: Silver Spring, MD: National Oceanic and Atmospheric Administration, National ….

A model-based investigation of the recent rebound of shelf water salinity in the Ross Sea

Jingwei Zhang [1,2], Xuebin Zhang[1], Matt A. King [2,3] and Kewei Lyu[4]

[1]Climate Science Centre, CSIRO Environment, Hobart, Australia

[2]School of Geography, Planning, and Spatial Sciences, University of Tasmania, Hobart, Australia

[3]The Australian Centre for Excellence in Antarctic Science, University of Tasmania, Hobart, Australia

[4]State Key Laboratory of Marine Environmental Science, College of Ocean and Earth Sciences, Xiamen University, Xiamen, China

Abstract

Intense atmosphere-ocean-ice interactions in the Ross Sea play a vital role in global overturning circulation by supplying saline and dense shelf waters. Since the 1960s, freshening of the Ross Sea shelf water has led to a decline in Antarctic Bottom Water formation. Since the early 2010s, however, the salinity of the western Ross Sea has rebounded. This study adopts an ocean-sea ice model to investigate the causes of this salinity rebound. Model-based salinity budget analysis indicates that the salinity rebound was driven by increased brine rejection from sea ice formation, triggered by the nearly equal effects of local anomalous winds and surface heat flux. The local divergent wind anomalies promoted local sea ice formation by creating a thin ice area, while a cooling heat flux anomaly decreased the surface temperature, increasing sea ice production. This highlights the importance of understanding local climate variability in projecting future dense shelf water change.

Introduction

The Ross Sea provides the densest Dense Shelf Water (DSW, the precursor for Antarctic bottom water (AABW), Figure 1a) on its continental shelf and contributes approximately 25% of all AABW formation on the Antarctic shelf (Orsi et al., 2002). Water in the western Ross Sea shelf is particularly important for AABW formation due to its high salinity, resulting from local salt inputs produced during sea ice formation (Rusciano et al., 2013; Sansiviero et al., 2017; Aulicino et al., 2018), together with remote sources advected toward the western Ross Sea by coastal currents (Assmann & Timmermann, 2005; Jendersie et al., 2018).

In the western Ross Sea, sea ice is driven northward by the persistent, strong southerly katabatic winds. During the austral winter (April- October), this results in vigorous sea ice formation and brine release, which initiates the formation of high-salinity shelf water and determines its properties (Fusco et al., 2009; Rusciano et al., 2013; Morrison et al., 2023). Moreover, the ocean circulation on the Ross Sea continental shelf consists of two main inflows from the east driven by the easterly wind, the Antarctic Coastal Current and Antarctic Slope Current (Smith Jr et al., 2012). Thus, these westward inflows are essential in transporting fresher water from the upstream Amundsen Sea to the Ross Sea (Figure 1a), influencing the long-term variability of DSW salinity in the western Ross Sea (S. Jacobs et al., 2022).

Ocean measurements in the western Ross Sea have shown a significant decrease (~0.03 psu per dec) in DSW salinity from 1958 to 2008 (Jacobs & Giulivi, 2010), which is thought to be driven by enhanced Antarctic melting in the Amundsen Sea (Nakayama et al., 2014). Beginning in the early 2010s, however, the DSW salinity in the western Ross Sea experienced a sharp rebound, with values in 2018 comparable to those in the mid-late 1990s (Castagno et al., 2019). This salinity rebound contradicts the expectation that the ongoing increased ice-sheet mass loss in West Antarctica would continue to decrease rather than increase DSW salinity in the western Ross Sea (Jacobs & Giulivi, 2010). Silvano et al. (2020), based on in situ observations, linked this salinity recovery to the enhanced sea ice formation driven by weakened easterly winds from the Amundsen Sea. However, insufficient observations limit a more comprehensive analysis of the individual physical interactions among the atmosphere, ocean, and sea ice that influence salinity variations in the western Ross Sea. In this work, we used a well-tuned global ocean sea-ice model and designed perturbation experiments to isolate the response of shelf water salinity to various atmospheric forcing, aiming to unravel the cause of observed salinity rebound. Our study highlights the importance of integrating observational data with model studies.

2 Model and experiment design

2.1 In situ hydrographic data

The observational data used in this study were sourced from in-situ salinity observations by Castagno et al. (2019), covering the period from 1995 to 2018 with sampling during most summers within this period. Hydrographic measurements in Terra Nova Bay (defined by 74.25°–75.50° S, 163°–166° E) with station depths deeper than 800 m have been used. The region chosen is representative of DSW conditions in the western Ross Sea with a marked rebound since the early 2010s (Figure 1b, red line). To compare with observations, model results are sampled in the same area for those years in which the observation data were taken (Figure 1b black line).

2.2 Model description

We adopted the Australian Community Climate and Earth System Simulator – Ocean Model 2 (ACCESS-OM2) (Kiss et al., 2020) with a configuration of 1-degree horizontal resolution and 50 z^* vertical levels covering from the surface to 5363.5m depth. The atmospheric forcing derived from JRA55-do (Tsujino et al., 2018), including wind speed, air temperature and humidity, radiation, precipitations, and sea level pressure, are used to diagnose air–sea fluxes (wind stress, heat flux, and freshwater flux) through bulk formulae and interactive coupling between ocean and sea ice. Freshwater flux and heat flux are defined as positive downward (i.e., freshwater/heat gain by the ocean). In this study, ACCESS-OM2 is initialized from a state of rest, with temperature and salinity fields coming from the World Ocean Atlas 2013 v2 monthly climatology (WOA13; (Locarnini et al., 2013; Zweng et al., 2013)).

After a 200-year spin-up under repeated 1990-1991 JRA55-do forcing (Tsujino et al., 2018), the model reached quasi-equilibrium and was then forced with the 3-hourly JRA55-do interannual year forcing for 29 years from 1 January 1990 to 31 December 2018. Our analysis focuses on the recent period 2000–2018. In this study, we used annual data from both model simulations and observations to ensure a consistent comparison between the two of them. More detailed information on the model setup can be found in the Supporting Information.

2.3 Surface salinity budget analysis

To quantify the processes driving surface salinity anomalies in our simulation, we use the surface salinity budget terms diagnosed in the model. At the surface, the ocean salinity budget in a grid cell is given by:

$$\frac{\partial S}{\partial t} = -\nabla \cdot (\boldsymbol{u}S) + \nabla \cdot (K_{eddy}S) + \nabla \cdot (K_{small}S) + \frac{(E-P-R)S}{h} + \frac{\rho_I I(S-S_I)}{\rho_0 h} \quad (1)$$

where S is sea surface salinity, ∂S/∂t is the salinity tendency, h is the grid cell thickness, and **u** is the three-dimension velocity. K_{eddy} is the diffusion tensor for mesoscale mixing, and K_{small} represents vertical diffusion and other mixing processes smaller than eddies. E and P are the rates of evaporation and precipitation (positive upward), and R is river runoff and meltwater from Antarctica and Greenland. I is the rate of sea ice formation while S_I is sea ice salinity. ρ_o and ρ_I are the reference seawater density and sea ice density, respectively.

In ACCESS-OM2 model, ocean salt content is conserved in each grid cell within the expected numerical precision. The salinity budget in Eq. 1 states that the time tendency of salinity (left-hand side) equals all contributing terms (right-hand side), including salt convergences due to the oceanic processes (advection, the first term, and diffusion, the second and third term), evaporation minus precipitation, runoff and meltwater, and sea ice. We use these salinity budget terms to isolate the respective contributions of these processes to the salinity rebound in our perturbation experiment.

2.4 Experiment design

In this study, we designed three perturbation experiments to investigate the role of atmospheric forcing in the rebound of shelf water salinity in the western Ross Sea (Table in the Supporting Information). In the first experiment, the All-Vary experiment, the ACCESS-OM2 model is forced with prescribed atmospheric conditions taken from the JRA55-do 3-hourly forcing from 2010 to 2018. In the second experiment from 2010 to 2018, the Wind-Vary experiment, the wind forcing is the same as in the All-Vary experiment, and the rest of the atmospheric forcing is replaced by the 3-hourly climatological forcing (derived over the 2000-2010 base period). In the third experiment from 2010 to 2018, the All-Fixed experiment, all the atmospheric forcing is replaced by the climatological forcing (derived over the 2000-2010 base period). In ACCESS-OM2, the ocean and sea ice models are forced by the surface heat flux, freshwater flux, and wind stress calculated on-the-fly from prescribed atmospheric conditions and model states. The ongoing increased Antarctic meltwater is not expected to explain the observed rapid salinity rebound (Adusumilli et al., 2020). Other freshwater flux, including precipitation, evaporation, and runoff, has a minimal impact on the salinity in the western Ross Sea (Jacobs & Giulivi, 2010; Porter et al., 2019).

Therefore, changes in atmospheric forcing in the study region, are mainly from surface heat flux and wind stress. We then compared the Wind-Vary experiment versus the All-Fixed experiment to isolate the impact of wind stress and compared the All-Vary experiment versus the Wind-Vary experiment to isolate the shelf water salinity response to surface heat flux anomaly.

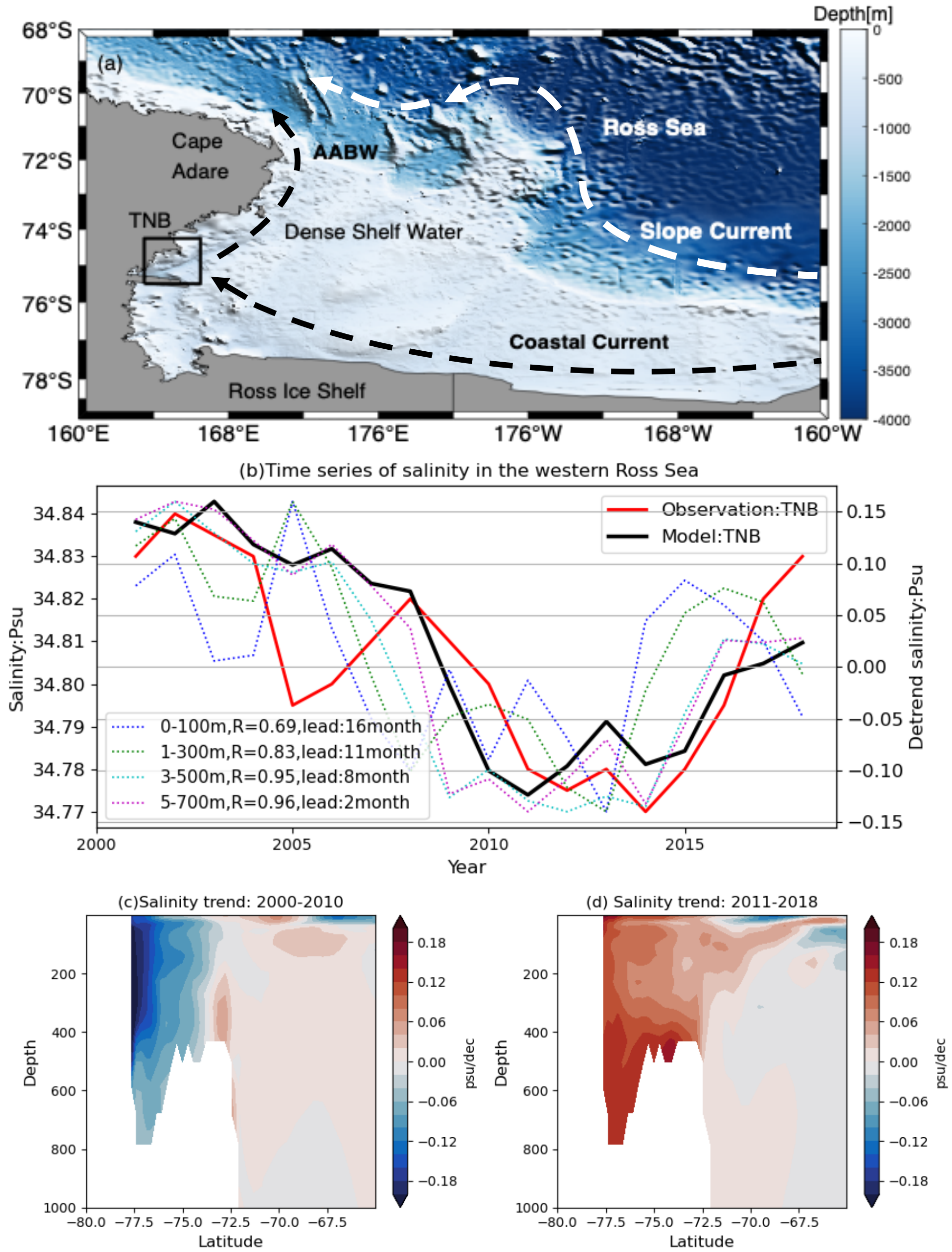

Figure 1 | Recent Recovery of DSW salinity in the Wester n Ross Sea. **(a)** Map of the Ross Sea and the study area in Terra Nova Bay (TNB, solid box). Bottom topography (m) is shown in color (Amante & Eakins, 2009). White and black dashed lines represent the general currents along the shelf break and on the shelf, referred to Smith et al. (2014). (**b**) Time series of averaged DSW salinity measured (solid red line) and simulated (solid black line) near the seafloor, as well as detrended model simulations at different depth ranges from surface to 700 m (dashed lines) and their leading correlations with salinity near the seafloor. Simulated zonal-averaged salinity trends from 2000-2010 (**c**) and 2011-2018 (**d**).

3. Results

3.1 Observed salinity variations in the western Ross Sea reproduced by model simulations

Figure 1 shows the map of the study area, and the observed and modelled salinities over different depth ranges in the western Ross Sea. The decreasing trend of DSW salinity near the seafloor before the early 2010s is estimated to be -0.05 psu/dec (Figure 1b, red line), slightly larger than the long-term trend of -0.03-0.04 psu/dec estimated by Jacobs et al. (2002) and Jacobs and Giulivi (2010). However, after reaching a minimum in the early 2010s, the freshening trend appears to reverse with a rapid salinity rebound (Figure 1b, red line). The DSW salinity in Terra Nova Bay (TNB) had rebounded up to 2018, reaching its value in the mid-late 1990s, indicating a recent recovery of DSW salinity in the western Ross Sea (Castagno et al., 2019). The observed decrease of DSW salinities between 2000 and the early 2010s followed by the sharp rebound is reproduced well by our model simulation based on ACCESS-OM2 (Figure 1b, red and black lines).

This recent sharp salinity rebound is simulated throughout the entire water column from surface to the bottom (Figures 1b, 1c,1d, and Figure S1 in Supporting Information), supported by a strong correlation, with surface salinity leading seafloor salinity at a maximum of 16 months ($r = 0.69$, $p<0.05$). We then discuss the drivers of the recent DSW salinity rebound since the early 2010s based on our model simulation.

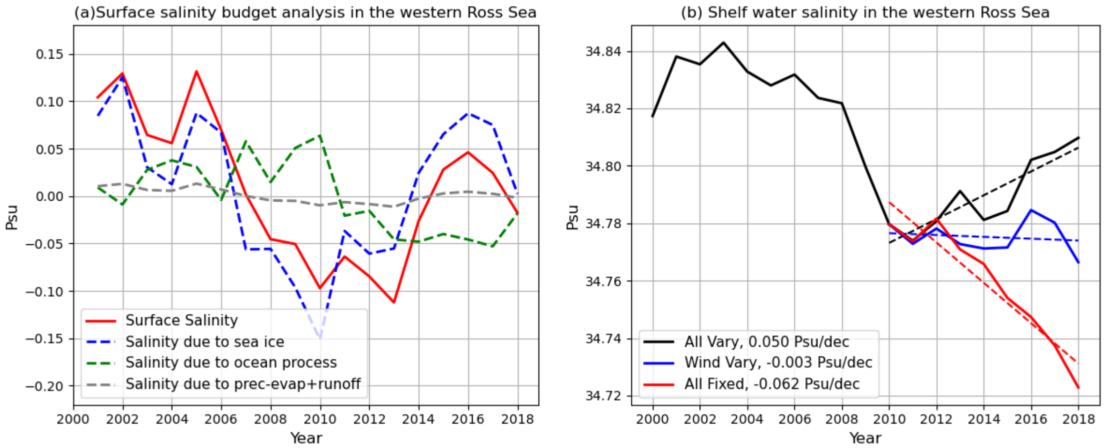

Figure 2 | Recent Recovery of DSW salinity induced by atmospheric forcing. (**a**) Time series of detrended model simulated surface salinity (red line) in western Ross Sea (162°E-168°E, 74°S-78°S), and time integrated surface salinity changes due to sea ice (bule line), net precipitation plus runoff (grey line) and oceanic process (green line) from 2000 to 2018. (**b**) Time series of averaged DSW salinity simulated by All Vary (black line) from 2000 to 2018, Wind Vary (blue line) and All Fixed (red line) and their trends (dashed lines) from 2011 to 2018 near the seafloor in TNB. Trend values are given in the legend in Psu per decade.

3.2 The effects of atmospheric forcing on recent salinity rebound through sea ice formation

A surface salinity budget analysis based on our model simulation (Figure 2a) reveals that increased brine rejection from sea ice production largely drives the recent salinity rebound over the western Ross Sea between 2010 and 2018. Oceanic processes counteract the salinity tendency implied by sea ice brine rejection. Other freshwater sources, such as precipitation minus evaporation, runoff, and Antarctic meltwater, exert minimal impact and cannot explain the observed rapid DSW salinity rebound. This is substantiated by hydrographic measurements that neither support a reduced net precipitation over the Ross Sea continental shelf (Porter et al., 2019) nor evidence of a decline in freshwater inflow from the Amundsen Sea (Adusumilli et al., 2020).

To further determine which atmospheric forcing is responsible for the recent salinity rebound, we conduct three perturbation experiments: All-Fixed, Wind-Vary, and All-Vary (see Table in Supporting Information). In the All-Fixed experiment, with atmospheric forcing remaining fixed to its climatology from 2000 to 2010, a negative trend in the salinity of the DSW is simulated (-0.062 psu/dec from 2011 to 2018, red line in Figure 2b), which is roughly consistent with the declining trend observed from the 1990s to the early 2010s (Jacobs & Giulivi, 2010; Castagno et al., 2019). The All-Fixed experiment suggests that a continued decrease in DSW salinity would be expected in the absence of changes in atmospheric conditions. The Wind-Vary experiment suggests that incorporating real-time wind forcing could basically stop the gradual decrease trend in salinity observed previously over 2000-2010 and stabilize without any obvious trends over 2010-2018 (blue line in Figure 2b). It is important to note that besides wind stress, other atmospheric factors also play a role in sea ice formation. Sea ice formation is closely connected to surface air temperature and sea surface temperature, which, in turn, is influenced by various types of surface heat flux from the atmosphere (Turner et al., 2015; Alekseev et al., 2022).

The All-Vary experiments provide compelling evidence that including all the real-time atmospheric forcing results in a notable rebound in DSW salinity in the western Ross Sea of +0.050 psu/dec over 2010- 2018, close to observations (Figure 2b, black line). Therefore, our model experiments suggest that the dynamic effect (sea ice formation driven by wind stress anomaly) and thermodynamic effect (sea ice formation driven by surface heat flux anomaly) have comparable impacts on the recent rebound in DSW salinity, contributing ~ 0.050 psu/dec each to the rebound (Figure 2b).

We next show the processes and mechanisms that how wind forcing (as revealed by comparing Wind-Vary and All-Fixed experiments) and surface heat flux (as revealed by comparing All-Vary and Wind-Vary experiments) cause increased sea ice production that further induces the recent rebound of DSW salinity in the western Ross Sea.

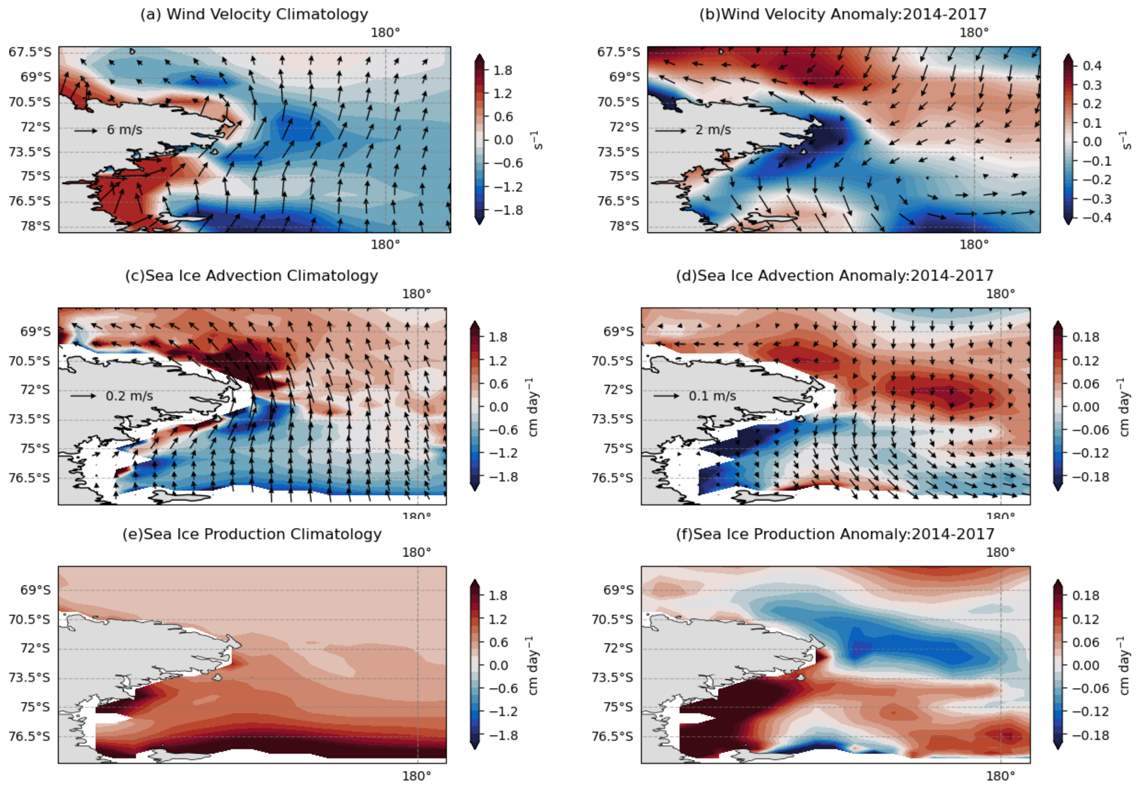

Figure 3 | Increased sea ice production due to sea ice divergence induced by wind anomalies. Climatology and 2014-2017 anomalies of winds (**a**,**b**, vectors, with colour shading represents wind divergence; negative values denote divergent), sea advection [-∇•**u***h*)] (**c**,**d**, sea ice motion and sea ice mass advection), and sea ice production (**e**,**f**) induced by wind forcing.

3.3 Increased sea ice formation driven by anomalous wind forcing

Sea ice dynamical processes, such as a changed sea ice motion in response to changing surface wind stress, play an important role in the redistribution of sea ice (Holland & Kwok, 2012; Turner et al., 2015). Ice motion is described by ice velocity, whereas sea ice advection is described here by sea ice convergence [-∇•(**u***h*)] (Figures 3c and 3d), where **u** is sea ice velocity and *h* is sea ice thickness (Zhang et al., 2010). Thus, changes in ice thickness (mass gain or loss) due to ice advection quantitatively describe the impact of wind-driven ice motion on sea ice spatial redistribution.

Mass loss due to sea ice advection generally occurs in the south region of the western Ross Sea, and ice gain occurs in the north (Figure 3c), indicating a sea ice motion from south to north in the Western Ross Sea (Comiso et al., 2011; Holland & Kwok, 2012; Turner et al., 2015). Such a sea ice advection pattern is attributed to strong northward ice motion driven by the coastal currents and strong southerly winds prevailing in winter (Holland & Kwok, 2012; Turner et al., 2016). During the period of 2014-2017, however, a local wind stress anomaly in the western Ross Sea displayed a divergent pattern (Figure 3b, blue shading). This anomaly had a notable impact on the motion of sea ice, particularly in impeding its northward motion, resulting in ice loss in the western Ross Sea (Figure 3d, blue shading, change in ocean circulation is negligible in our Wind-Vary experiment) and concurrent ice gain in the Ross Sea polynya near the coast (Figure 3d, red shading). Consequently, local changes in ice thickness (gain and loss) due to this reduced northward ice transport can be up to 0.2 cm/day, leading to the expansion of a larger area of thin ice in the north and a narrow area of thick ice near the coast (Figure S4). This increased presence of thin ice contributes to enhanced ice growth and brine rejection (Figure 3f), as growth rates of thin ice are higher compared to thick ice (Zhang et al., 2010).

The significant negative spatial correlation between the simulated anomalies of sea ice advection and sea ice production (Figures 3d, 3f, $r = -0.73$, $p<0.01$) further highlights the close relationship between wind-driven sea ice mass advection and ice production. Additionally, the sea ice loss (gain) resulting from sea ice mass advection exhibits a significant correlation with the wind divergence anomaly over the western Ross Sea (Figures 3b and 3d, $r = 0.67$, $p<0.01$). These findings suggest that, in the Wind-Vary experiment, wind forcing plays a dominant role in the formation of ice in the Ross Sea, primarily through ice mass advection processes. To identify the region where the wind forcing is responsible for the changes in sea ice in the Western Ross Sea, we conducted further experiments (Supporting Information 1.4 and Figure S2). Our investigation reveals that only when applying real-time wind forcing in the western Ross Sea region (160ºE-170ºW, 60ºS-80ºS) the model is able to successfully simulate the increased salinity of DSW driven by wind (Figures S2 and S3). This suggests that the wind-driven component of the simulated increase in DSW salinity is primarily driven by local wind anomalies rather than non-local wind originating from distant regions. Thus, during the period of 2014-2017, the amplified sea ice production and brine rejection observed in the Wind-Vary experiment in the western Ross Sea can be attributed to the thinning of sea ice caused by local divergent wind anomalies.

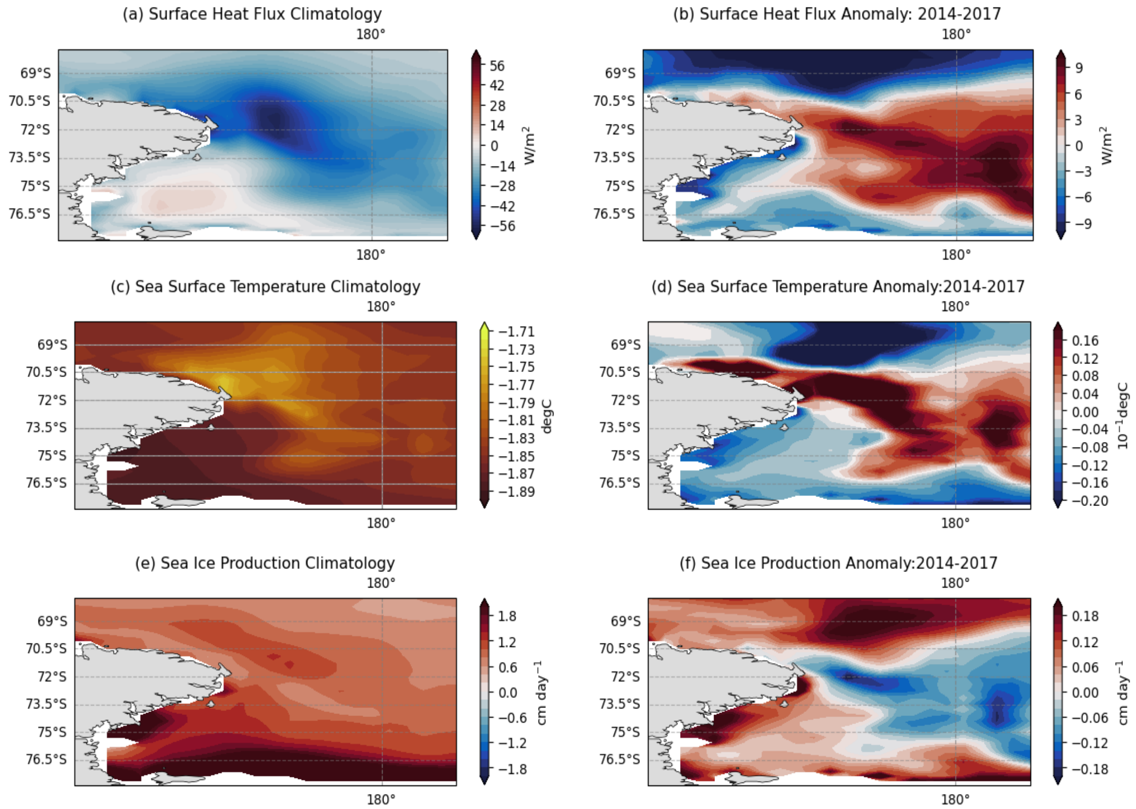

Figure 4 | Increased sea ice production due to lower temperatures induced by surface heat flux anomalies. Climatology and 2014-2017 anomalies of surface heat flux (Wm^{-2}; positive downward) (**a,b**), sea surface temperature (°C) (**c,d**) and sea ice production (cm/day) (**e,f**) induced by atmospheric forcing other than wind.

3.4 Increased sea ice formation driven by surface heat flux

In addition to the dynamical processes induced by wind, thermodynamic processes can also play an important role in the production of sea ice. During the sea ice growth season, the surface heat flux plays a crucial role in influencing sea ice production by affecting the sea surface temperature (Turner et al., 2015; Alekseev et al., 2022). During the period of 2014-2017, a comparison between All-vary and wind-vary model experiments reveals that with a decrease in surface heat flux from the atmosphere, there is a corresponding decrease in upper-ocean temperature (Figures 4b and 4d) in the western Ross Sea. This decrease in temperature promotes an increase in sea ice growth, resulting in increased brine rejection from the new ice and subsequently contributing to an increased salinity from surface to seafloor in the western Ross Sea (Figures 2b and 4f). The significant spatial correlation between the anomalies of surface heat flux and sea surface temperature (Figures 4b and 4d, $r = 0.68$, $p<0.01$), and sea ice production (Figures 4b and 4f, $r = 0.63$, $p<0.01$) further highlights the strong connection between surface heat flux and sea ice production.

It is essential to note that contrary to a simplistic inverse correlation, the relationship between sea surface temperature and net sea ice production is more intricate (Zhang, 2007). Our simulations indicate that in the upper 200 meters of the western Ross Sea, an increase in salinity and a decrease in temperature lead to increased ocean density (Figure S5). This increased upper-ocean density in turn reduces stratification (the denser layer above the lighter layer) and enhances vertical heat exchange, leading to a greater upward ocean heat transport available to melt the sea ice (Zhang, 2007; Turner et al., 2015). The pivotal balance of sea ice thus lies between the initial sea ice growth driven by surface cooling and the sea ice melt induced by vertical heat flux from the subsurface. In line with this, our model exhibits a positive anomaly in local net ice production of 0.2 cm/day (Figure 4f), primarily driven by a more pronounced increase in ice growth compared to ice melt (Figure S6). Hence, the overall increase in net sea ice production and brine rejection due to the thermodynamic process is driven by the rate of ice growth—induced by lower surface temperatures— surpassing the rate of ice melt, which itself is influenced by increased convective overturning and resultant upward ocean heat transport.

4. Discussion and conclusions

This study presents results from a model study of the recent rebound of DSW salinity in the western Ross Sea. Sea surface salinity budget analysis shows that the recent salinity rebound is dominated by increased brine rejection from sea ice formation, which further propagates and extends the whole water column from surface to seafloor (0-900 m). We further conduct three model perturbation experiments and find that this increased sea ice formation is driven by the combined effect of anomalous local wind stress and surface heat flux, which have nearly equal impacts on shelf water salinity rebound through dynamic and thermodynamic processes. During 2014-2017, the local wind anomalies induced a divergent motion in sea ice, reducing sea ice thickness and promoting local sea ice formation. Meanwhile, cooling heat flux anomaly from the atmosphere cools the surface, increasing sea ice production in winter.

The Southern Oscillation Index (SOI) captures variability associated with the ENSO events, influencing the low-pressure system over the Amundsen Sea (Amundsen Sea Low, ASL) through the atmospheric teleconnection (Lee & Jin, 2023). A negative SOI (corresponding to an El Niño event) over 2014-2017 (Figure S7a) influenced an eastward and northward shift of the ASL central (Figure S7b) (Raphael et al., 2016), leading to a reduction in the meridional sea level pressure gradient in the western Ross Sea (Figures S7 c,d) (Coggins & McDonald, 2015), thus weakening southerlies and reducing surface heat flux in the western boundary (Clem et al., 2017), ultimately leading to the recent rebound of DSW salinity through sea ice formation.

Long-term observations have recorded a freshening AABW over the past 60 years (Jacobs & Giulivi, 2010; Silvano et al., 2018), as a result of increased Antarctic meltwater (Lago & England, 2019; Johnson, 2022). Our study reveals that climate variability can temporally counteract this long-term freshening by enhancing sea ice formation and brine rejection. Future climate projections show an increased frequency of extreme El Niño events due to the greenhouse warming (Cai et al., 2014), therefore possibly enhancing AABW formation that potentially offsets or even surpasses the meltwater-induced freshening on different time scales. Thus, the experiment design and salinity budget analysis conducted here provide an essential reference for identifying the major drivers of the shelf water salinity variations from interannual to decadal time scales.

Acknowledgments

This research was supported by the Australian Research Council Special Research Initiative, the Australian Centre for Excellence in Antarctic Science (Project Number SR200100008), and the Centre for Southern Hemisphere Oceans Research (CSHOR), jointly funded by the Commonwealth Scientific and Industrial Research Organisation (CSIRO, Australia) and the Qingdao National Laboratory for Marine Science and Technology (QNLM, China). This research was undertaken with the assistance of resources from the National Computational Infrastructure (NCI Australia). The authors thank the Consortium for Ocean-Sea Ice Modelling in Australia (COSIMA; http://www.cosima.org.au) for making the ACCESS-OM2 suite of models available at https://github.com/COSIMA/access-om2.

Data Availability Statement

The observational data used in this study were sourced from in-situ salinity observations by Castagno et al. (2019), covering the period from 1995 to 2018. The model source code is available from https://github.com/COSIMA/access-om2/. The configuration files for the repeat year forced simulation are available from https://github.com/COSIMA/1deg_jra55_ryf and for the interannually forced simulation from https://github.com/COSIMA/1deg_jra55_iaf Mode experiment and outputs are available from the Zenodo repository at https://doi.org/10.5281/zenodo.8415955

Reference

Adusumilli, S., Fricker, H. A., Medley, B., Padman, L., & Siegfried, M. R. (2020). Interannual variations in meltwater input to the Southern Ocean from Antarctic ice shelves. *Nature Geoscience, 13*(9), 616-620.

Alekseev, G., Vyazilova, A., & Smirnov, A. (2022). Influence of Sea Surface Temperature in the Tropics on the Antarctic Sea Ice during Global Warming. *Journal of Marine Science and Engineering, 10*(12), 1859.

Amante, C., & Eakins, B. W. (2009). ETOPO1 arc-minute global relief model: procedures, data sources and analysis.

Assmann, K. M., & Timmermann, R. (2005). Variability of dense water formation in the Ross Sea. *Ocean Dynamics, 55*(2), 68-87.

Aulicino, G., Sansiviero, M., Paul, S., Cesarano, C., Fusco, G., Wadhams, P., & Budillon, G. (2018). A new approach for monitoring the Terra Nova Bay polynya through MODIS ice surface temperature imagery and its validation during 2010 and 2011 winter seasons. *Remote Sensing, 10*(3), 366.

Cai, W., Borlace, S., Lengaigne, M., Van Rensch, P., Collins, M., Vecchi, G., et al. (2014). Increasing frequency of extreme El Niño events due to greenhouse warming. *Nature Climate Change, 4*(2), 111-116.

Castagno, P., Capozzi, V., DiTullio, G. R., Falco, P., Fusco, G., Rintoul, S. R., et al. (2019). Rebound of shelf water salinity in the Ross Sea. *Nature communications, 10*(1), 1-6.

Clem, K. R., Renwick, J. A., & McGregor, J. (2017). Large-scale forcing of the Amundsen Sea low and its influence on sea ice and West Antarctic temperature. *Journal of Climate, 30*(20), 8405-8424.

Coggins, J. H., & McDonald, A. J. (2015). The influence of the Amundsen Sea Low on the winds in the Ross Sea and surroundings: Insights from a synoptic climatology. *Journal of Geophysical Research: Atmospheres, 120*(6), 2167-2189.

Comiso, J. C., Kwok, R., Martin, S., & Gordon, A. L. (2011). Variability and trends in sea ice extent and ice production in the Ross Sea. *Journal of Geophysical Research: Oceans, 116*(C4).

Fusco, G., Budillon, G., & Spezie, G. (2009). Surface heat fluxes and thermohaline variability in the Ross Sea and in Terra Nova Bay polynya. *Continental Shelf Research, 29*(15), 1887-1895.

Holland, P. R., & Kwok, R. (2012). Wind-driven trends in Antarctic sea-ice drift. *Nature Geoscience, 5*(12), 872-875.

Jacobs, & Giulivi. (2010). Large multidecadal salinity trends near the Pacific–Antarctic continental margin. *Journal of Climate, 23*(17), 4508-4524.

Jacobs, Giulivi, & Mele, P. (2002). Freshening of the Ross Sea during the late 20th century. *Science, 297*(5580), 386-389.

Jacobs, S., Giulivi, C., & Dutrieux, P. (2022). Persistent Ross Sea freshening from imbalance West Antarctic ice shelf melting. *Journal of Geophysical Research: Oceans, 127*(3), e2021JC017808.

Jendersie, S., Williams, M. J., Langhorne, P. J., & Robertson, R. (2018). The density‐driven winter intensification of the Ross Sea circulation. *Journal of Geophysical Research: Oceans, 123*(11), 7702-7724.

Johnson, G. C. (2022). Antarctic Bottom Water Warming and Circulation Slowdown in the Argentine Basin From Analyses of Deep Argo and Historical Shipboard Temperature Data. *Geophysical Research Letters, 49*(18), e2022GL100526.

Kiss, A. E., Hogg, A. M., Hannah, N., Boeira Dias, F., Brassington, G. B., Chamberlain, M. A., et al. (2020). ACCESS-OM2 v1. 0: a global ocean–sea ice model at three resolutions. *Geoscientific Model Development, 13*(2), 401-442.

Lago, V., & England, M. H. (2019). Projected slowdown of Antarctic bottom water formation in response to amplified meltwater contributions. *Journal of Climate, 32*(19), 6319-6335.

Lee, H.-J., & Jin, E. K. (2023). Understanding the delayed Amundsen Sea low response to ENSO. *Frontiers in Earth Science, 11*, 1136025.

Locarnini, R., Mishonov, A., Antonov, J., Boyer, T., Garcia, H., Baranova, O., et al. (2013). World Ocean Atlas 2013, Volume 1: Temperature in: NOAA Atlas NESDIS 73 edited by S. In: Levitus.

Morrison, A. K., Huneke, W. G., Neme, J., Spence, P., Hogg, A. M., England, M. H., & Griffies, S. M. (2023). Sensitivity of Antarctic shelf waters and abyssal overturning to local winds. *Journal of Climate*, 1-32.

Nakayama, Y., Timmermann, R., Rodehacke, C. B., Schröder, M., & Hellmer, H. H. (2014). Modeling the spreading of glacial meltwater from the Amundsen and Bellingshausen Seas. *Geophysical Research Letters, 41*(22), 7942-7949.

Orsi, A. H., Smethie Jr, W. M., & Bullister, J. L. (2002). On the total input of Antarctic waters to the deep ocean: A preliminary estimate from chlorofluorocarbon measurements. *Journal of Geophysical Research: Oceans, 107*(C8), 31-31-31-14.

Porter, D. F., Springer, S. R., Padman, L., Fricker, H. A., Tinto, K. J., Riser, S. C., et al. (2019). Evolution of the seasonal surface mixed layer of the Ross Sea, Antarctica, observed with autonomous profiling floats. *Journal of Geophysical Research: Oceans, 124*(7), 4934-4953.

Raphael, M. N., Marshall, G., Turner, J., Fogt, R., Schneider, D., Dixon, D., et al. (2016). The Amundsen Sea low: Variability, change, and impact on Antarctic climate. *Bulletin of the American Meteorological Society, 97*(1), 111-121.

Rusciano, E., Budillon, G., Fusco, G., & Spezie, G. (2013). Evidence of atmosphere–sea ice–ocean coupling in the Terra Nova Bay polynya (Ross Sea—Antarctica). *Continental Shelf Research, 61*, 112-124.

Sansiviero, M., Maqueda, M. M., Fusco, G., Aulicino, G., Flocco, D., & Budillon, G. (2017). Modelling sea ice formation in the Terra Nova Bay polynya. *Journal of Marine Systems, 166*, 4-25.

Silvano, A., Foppert, A., Rintoul, S. R., Holland, P. R., Tamura, T., Kimura, N., et al. (2020). Recent recovery of Antarctic Bottom Water formation in the Ross Sea driven by climate anomalies. *Nature Geoscience, 13*(12), 780-786.

Silvano, A., Rintoul, S. R., Peña-Molino, B., Hobbs, W. R., van Wijk, E., Aoki, S., et al. (2018). Freshening by glacial meltwater enhances melting of ice shelves and reduces formation of Antarctic Bottom Water. *Science Advances, 4*(4), eaap9467.

Smith Jr, W. O., Sedwick, P. N., Arrigo, K. R., Ainley, D. G., & Orsi, A. H. (2012). The Ross Sea in a sea of change. *Oceanography, 25*(3), 90-103.

Smith, W. O., Dinniman, M. S., Hofmann, E. E., & Klinck, J. M. (2014). The effects of changing winds and temperatures on the oceanography of the Ross Sea in the 21st century. *Geophysical Research Letters, 41*(5), 1624-1631.

Tsujino, H., Urakawa, S., Nakano, H., Small, R. J., Kim, W. M., Yeager, S. G., et al. (2018). JRA-55 based surface dataset for driving ocean–sea-ice models (JRA55-do). *Ocean Modelling, 130*, 79-139.

Turner, J., Hosking, J. S., Bracegirdle, T. J., Marshall, G. J., & Phillips, T. (2015). Recent changes in Antarctic sea ice. *Philosophical Transactions of the Royal Society A: Mathematical, Physical and Engineering Sciences, 373*(2045), 20140163.

Turner, J., Hosking, J. S., Marshall, G. J., Phillips, T., & Bracegirdle, T. J. (2016). Antarctic sea ice increase consistent with intrinsic variability of the Amundsen Sea Low. *Climate Dynamics, 46*, 2391-2402.

Zhang, J. (2007). Increasing Antarctic sea ice under warming atmospheric and oceanic conditions. *Journal of Climate, 20*(11), 2515-2529.

Zhang, J., Woodgate, R., & Moritz, R. (2010). Sea ice response to atmospheric and oceanic forcing in the Bering Sea. *Journal of Physical Oceanography, 40*(8), 1729-1747.

Zweng, M., Reagan, J., Antonov, J., Locarnini, R., Mishonov, A., Boyer, T., et al. (2013). World Ocean atlas 2013. Vol. 2. Salinity. NOAA Atlas NESDIS 74. In: Silver Spring, MD: National Oceanic and Atmospheric Administration, National ….

AGU PUBLICATIONS

Geophysical Research Letters

Supporting Information for

A model-based investigation of the recent rebound of shelf water salinity in the Ross Sea

Jingwei Zhang [1,2], Xuebin Zhang[1], Matt A. King [2,3], Kewei Lyu[4]

[1]Climate Science Centre, CSIRO Environment, Hobart, Australia

[2]School of Geography, Planning, and Spatial Sciences, University of Tasmania, Hobart, Australia

[3]The Australian Centre for Excellence in Antarctic Science, University of Tasmania, Hobart, Australia

[4]State Key Laboratory of Marine Environmental Science, College of Ocean and Earth Sciences, Xiamen University, Xiamen, China

Overview

We present here additional information related to oceanography data, model simulation setup, summary of perturbation experiment settings, and the additional experiment and analysis (Figures S1 to S7).

Contents of this file

1. Method

2. Table

3. Figures S1 to S7

3. Figures

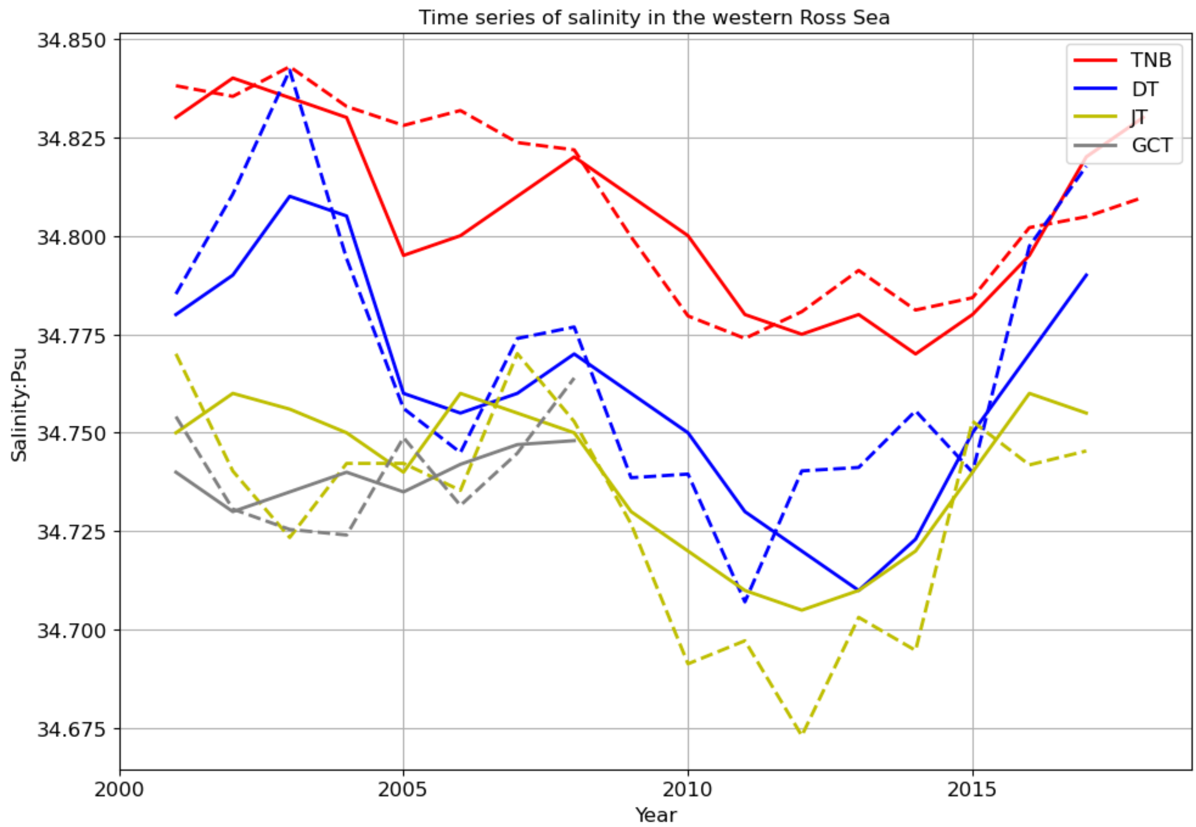

Figure S1 | Comparisons of salinity between model experiments and observations. Time series of averaged DSW salinity measured (solid line) and model-simulated (dashed line) near the seafloor at Terra Nova Bay (TNB, red line), Drygalski Trough mouth (DT, blue line), Joides Trough (JT, yellow line) and Glomar Challenger Trough (GCT, grey line) from 2000 to 2018.

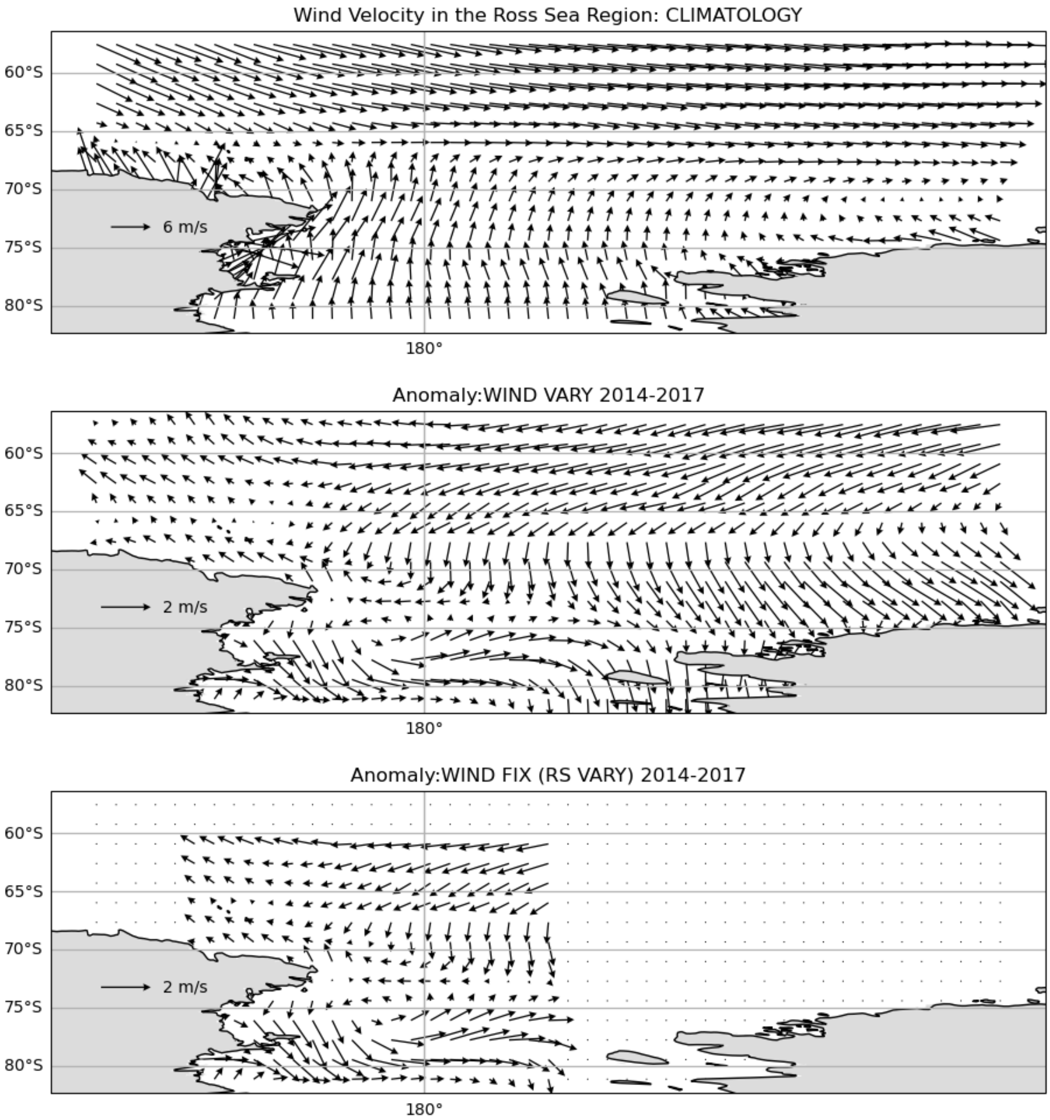

Figure S2 | Interannual variability of winds in the western Ross Sea. The Ross Sea-Only simulation employed a fixed wind forcing and real-time other atmospheric forcing approach for the entire Southern Ocean, except for the western Ross Sea (160^{o}E-170^{o}W, 60^{o}S-80^{o}S), where real-time wind forcing was implemented.

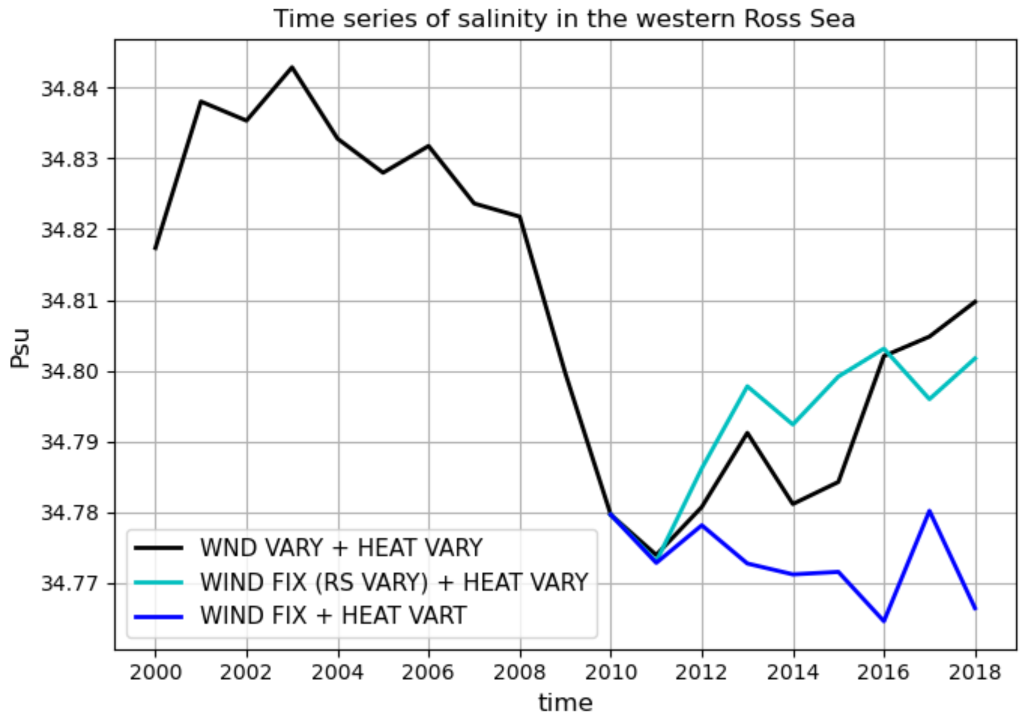

Figure S3 | Simulated DSW salinity from further perturbation experiments Time series of averaged DSW salinity simulated by All Vary (black line) from 2000 to 2018, Wind Fix (Ross Sea Wind Vary) + Heat Vary (cyan line) and Wind Fix + Heat Vary (blue line) from 2010 to 2018 near the seafloor in TNB (details in Supplementary 1.4. Ross Sea-only wind experiment).

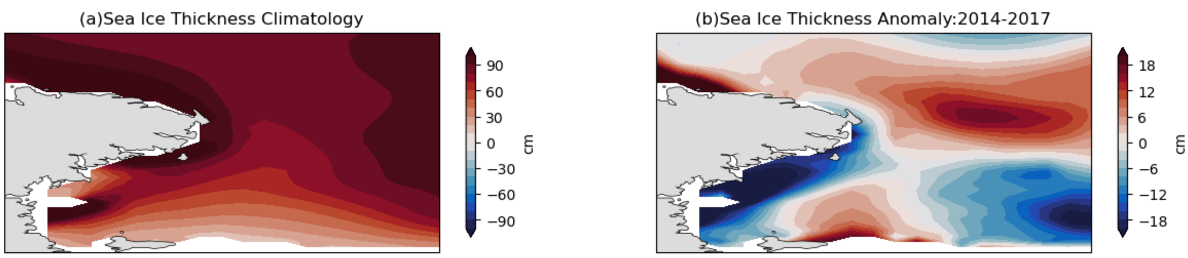

Figure S4 | Sea ice thickness in wind experiment. Climatology (**a,** All-Fixed) and 2014-2017 anomaly (**b,** Wind-Vary minus All-Fixed) of sea ice thickness induced by wind forcing.

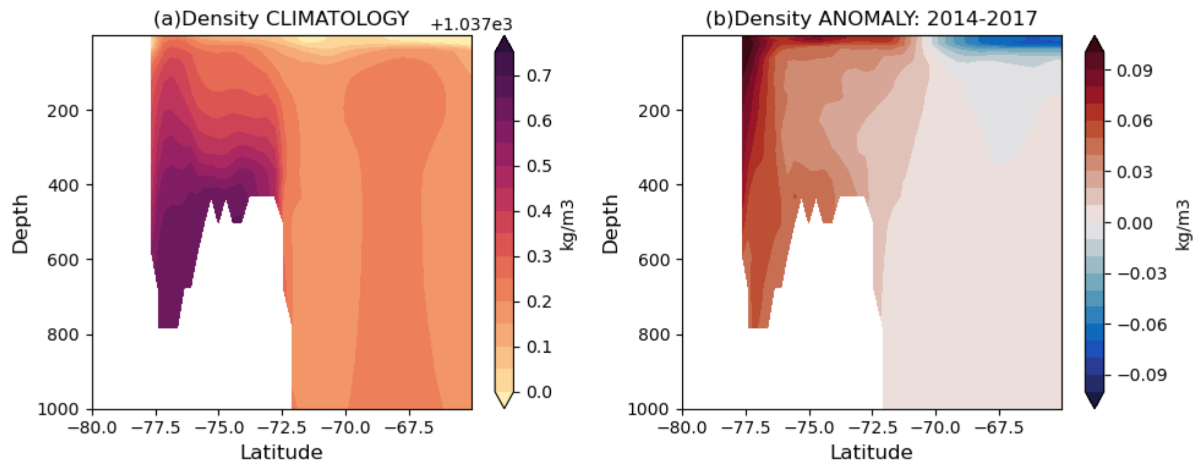

Figure S5 | Density change in surface heat flux experiment. Zonal averaged climatology (**a**, Wind-Vary) and 2014-2017 anomaly (**b**, All-Vary minus Wind-Vary) of ocean density in heat flux experiment.

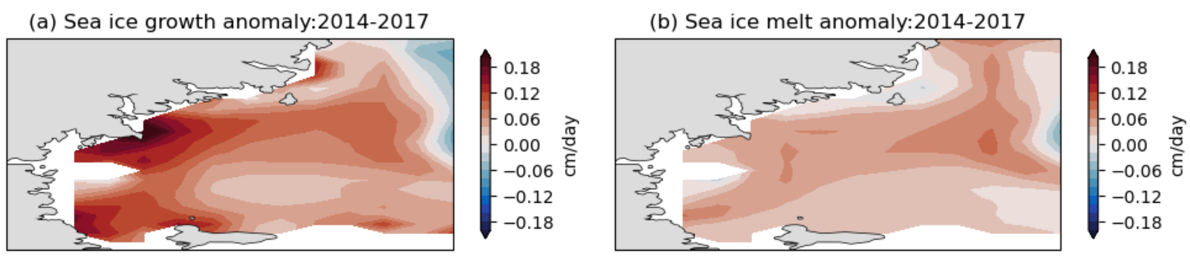

Figure S6 | Sea ice growth and melt in surface heat flux experiment. Averaged sea ice anomalies (All-Vary minus Wind-Vary) in growth (**a**) and melt (**b**) between 2014 to 2017 in heat flux experiment.

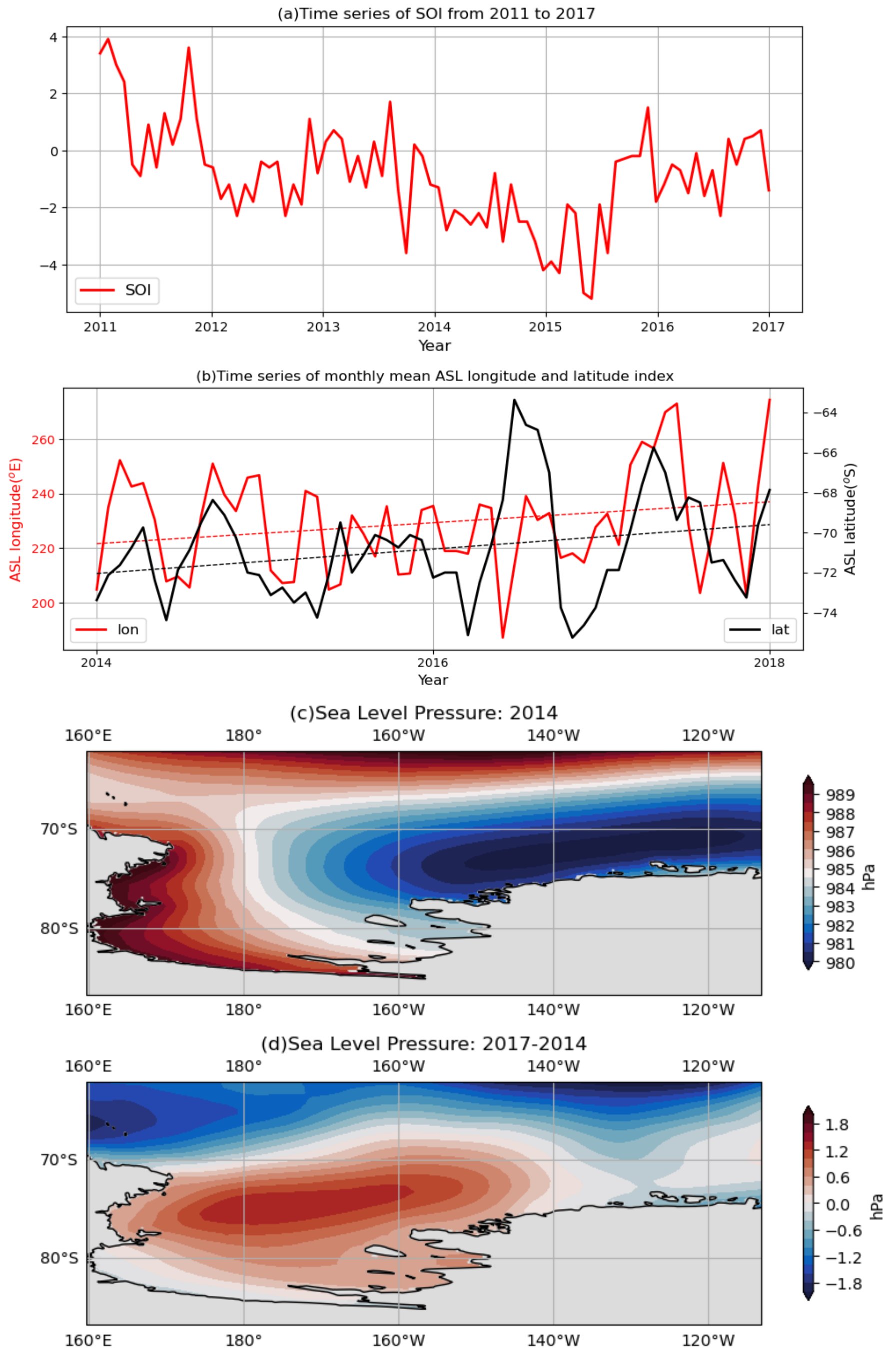

Figure S7 | Wind forcing, and surface heat flux driven by climate anomalies. (**a**) Time series of SOI between 2011 to 2018. The period from 2014-2017 is characterized by negative SOI. (**b**) Time series (solid line) and trends (dashed line) of ASL central latitude (black line) and longitude (red line) from 2014-2018, within the ASL sector (170°E-298° E, 80°S-60° S). Sea level pressure in 2014 (**c**), and anomaly in 2017 (**d**).

AGU PUBLICATIONS

Geophysical Research Letters

Supporting Information for

A model-based investigation of the recent rebound of shelf water salinity in the Ross Sea

Jingwei Zhang [1,2], Xuebin Zhang[1], Matt A. King [2,3], Kewei Lyu[4]

[1]Climate Science Centre, CSIRO Environment, Hobart, Australia

[2]School of Geography, Planning, and Spatial Sciences, University of Tasmania, Hobart, Australia

[3]The Australian Centre for Excellence in Antarctic Science, University of Tasmania, Hobart, Australia

[4]State Key Laboratory of Marine Environmental Science, College of Ocean and Earth Sciences, Xiamen University, Xiamen, China

Overview

We present here additional information related to oceanography data, model simulation setup, summary of perturbation experiment settings, and the additional experiment and analysis (Figures S1 to S7).

Contents of this file

1. Method

2. Table

3. Figures S1 to S7

2. Table | Summary of experiment simulation settings

Simulation	Wind forcing	Other atmospheric forcing
All Vary	Interannual	Interannual
Wind Vary	Interannual	Climatology
All Fixed	Climatology	Climatology

Note that ‘Interannual’ represents real-time atmospheric forcing, and ‘Climatology’ represents the averaged atmospheric condition from 2000 to 2010.

AGU PUBLICATIONS

Geophysical Research Letters

Supporting Information for

A model-based investigation of the recent rebound of shelf water salinity in the Ross Sea

Jingwei Zhang [1,2], Xuebin Zhang[1], Matt A. King [2,3], Kewei Lyu[4]

[1]Climate Science Centre, CSIRO Environment, Hobart, Australia

[2]School of Geography, Planning, and Spatial Sciences, University of Tasmania, Hobart, Australia

[3]The Australian Centre for Excellence in Antarctic Science, University of Tasmania, Hobart, Australia

[4]State Key Laboratory of Marine Environmental Science, College of Ocean and Earth Sciences, Xiamen University, Xiamen, China

Overview

We present here additional information related to oceanography data, model simulation setup, summary of perturbation experiment settings, and the additional experiment and analysis (Figures S1 to S7).

Contents of this file

1. Method

2. Table

3. Figures S1 to S7

1. Method

1.1 Oceanography data

The oceanographic data utilized in this study were sourced from the work of Castagno et al. (2019). To capture the salinity changes in the Deep Shelf Water (DSW) of the Ross Sea, specific regions were selected for analysis. The time series in Fig.1a and Supplementary S1 were obtained by averaging the salinity in the 30 dbar layer from 870 to 900 dbar for TNB (74.25°S–75.50°S and 163.00°E–166.00°E), and in the bottom 20 dbar for Drygalski Trough mouth (DT, 72.00°S and 72.67°S and 171.50°E and 174.50°E), Joides Trough (JT, 73.90°S–74.10°S and 174.20° E–176.00°E) and Glomar Challenger Trough (GCT, 75.80°S–76.20°S and 178.00°W–177.10°W).

1.2 Climate indices

The Southern Oscillation Index (SOI) captures variability associated with the El Niño/La Niña cycle and represents the dominant modes of atmospheric variability in the Pacific sector of the Southern Ocean. We used monthly SOI provided by NCAR (https://climatedataguide.ucar.edu/climate-data/southern-oscillation-indices-signal-noise-and-tahitidarwin-slp-soi). The monthly location of ASL central was also used in this study, sourced from (https://scotthosking.com/asl_index). The location of ASL central, which is the minimum sea surface pressure, is defined using an ASL detection methodology, described in (Hosking et al., 2016).

1.3 Model simulation setup

ACCESS-OM2 is a global model with coupled ocean and sea-ice components driven by prescribed atmosphere forcing. The ocean component is the Modular Ocean Model version 5.1 (MOM5.1; (Griffies, 2012) from the National Oceanic and Atmospheric Administration Geophysical Fluid Dynamics Laboratory (NOAA-GFDL). The sea-ice component is the

Community Ice Code version 5.1.2 (CICE5.1.2;(Hunke et al., 2015)). The coupling of these two components is achieved by the model coupling toolkit from CERFACS and CNRA through the Ocean Atmospheric Sea Ice Soil version 3 (OASIS3; (Valcke, 2006)). ACCESS-OM2 simulation is initialized from rest with zero sea level and with temperature and salinity from the World Ocean Atlas 2013 (WOA13). Surface salinity was restored to the WOA13 monthly climatology with a restoring time scale of 21days over the top layer.

The initial phase of our study involves a 200-year spin-up, which is driven by the repeat year forcing from 1st May 1990 through 30th April 1991 (RYF-9091, repeat-year forcing 1990-1991). This repeat year forcing is chosen due to its neutral characteristics with respect to major climate variability modes. Following this spin-up, the ACCESS-OM2 model is then forced with interannually varying atmospheric variables based on the Japanese 55-Year Reanalysis (JRA-55) dataset for driving ocean–sea ice models version 1.4 (hereafter referred to as JRA55-do v1.4; (Tsujino et al., 2018)) from 1990 to 2018.

1.4 Experiment design: Ross Sea-only wind experiment

To ascertain the specific location of the wind responsible for the changes in sea ice, we conducted further experiments called the Ross Sea-only wind experiment. The Ross Sea-only simulation employed a fixed wind forcing (climatology) and real-time other atmospheric forcing approach for the entire Southern Ocean, except for the western Ross Sea (160^{o}E-170^{o}W, 60^{o}S-80^{o}S), where real-time wind forcing was implemented. We then compared the Ross Sea-only wind experiment versus the heat-vary experiment (climatological wind forcing and real-time other atmospheric forcing) to isolate the impact of local wind stress anomaly in the western Ross Sea.

Supplementary References

Castagno, P., Capozzi, V., DiTullio, G. R., Falco, P., Fusco, G., Rintoul, S. R., et al. (2019). Rebound of shelf water salinity in the Ross Sea. *Nature communications, 10*(1), 1-6.

Griffies, S. M. (2012). Elements of the modular ocean model (MOM). *GFDL Ocean Group Tech. Rep, 7*(620), 47.

Hosking, J. S., Orr, A., Bracegirdle, T. J., & Turner, J. (2016). Future circulation changes off West Antarctica: Sensitivity of the Amundsen Sea Low to projected anthropogenic forcing. *Geophysical Research Letters, 43*(1), 367-376.

Hunke, E., Lipscomb, W., Turner, A., Jeffery, N., & Elliott, S. (2015). CICE: The Los Alamos Sea ice Model Documentation and Software User's Manual Version 5 (Tech. Rep. LA-CC-06–012). *Los Alamos, NM: Los Alamos National Laboratory*.

Tsujino, H., Urakawa, S., Nakano, H., Small, R. J., Kim, W. M., Yeager, S. G., et al. (2018). JRA-55 based surface dataset for driving ocean–sea-ice models (JRA55-do). *Ocean Modelling, 130*, 79-139.

Valcke, S. (2006). *OASIS User guide, prism 2-5, PRISM-Support Initiative*. Retrieved from